Nano Research

ISSN 1998-0124 CN 11-5974/O4
https://doi.org/10.26599/NR.2026.94909100

Research Article

Chemical mechanical polishing on silicon carbide using developed ceria composite abrasives and their synergistic polishing mechanism

Juan Liang[1,§], Yan Zhang[1,§], Zhaokang Li[1], Peng Lv[1], Wenhao Qi[1], Hong Feng[1], Xuan Xu[1,2](✉), Baocang Liu[1,2], Tao Bai[3], Peng Jing[1,2](✉), Jun Zhang[1,4](✉)

[1] School of Chemistry and Chemical Engineering, Inner Mongolia University, 49 Xilinguole South Road, Hohhot 010020, China

[2] Inner Mongolia Key Laboratory of Rare Earth Catalysis, Inner Mongolia University, 49 Xilinguole South Road, Hohhot 010020, China

[3] Inner Mongolia Guangheyuan Nano High Tech Co., Ltd., 22 Sarula North Road, Ordos 017010, China

[4] School of Chemistry and Environmental Science, Inner Mongolia Normal University, 81 Zhaowuda Road, Hohhot 010022, China

[§] Juan Liang and Yan Zhang contributed equally to this work.

Nano Res., **Just Accepted Manuscript** • https://doi.org/10.26599/NR.2026.94909100

https://www.sciopen.com/journal/1998-0124 on Aug. 10, 2026

TABLE OF CONTENTS (TOC)

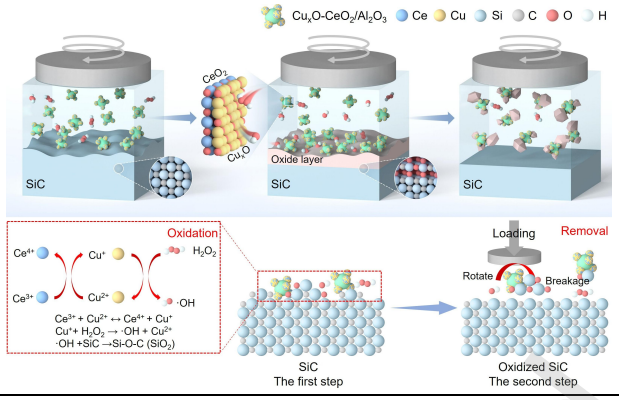

By employing Cu_xO-CeO_2 as the catalyst for Fenton-like H_2O_2 decomposition, the polishing performance of Al_2O_3 abrasives for SiC is significantly enhanced through a synergistic chemical oxidation and mechanical abrasion.

Nano Research

Open Access

Research Article

Chemical mechanical polishing on silicon carbide using developed ceria composite abrasives and their synergistic polishing mechanism

Juan Liang[1,§], Yan Zhang[1,§], Zhaokang Li[1], Peng Lv[1], Wenhao Qi[1], Hong Feng[1], Xuan Xu[1,2] ✉, Baocang Liu[1,2], Tao Bai[3], Peng Jing[1,2] ✉, and Jun Zhang[1,4] ✉

[1] *School of Chemistry and Chemical Engineering, Inner Mongolia University, 49 Xilinguole South Road, Hohhot 010020, China*
[2] *Inner Mongolia Key Laboratory of Rare Earth Catalysis, Inner Mongolia University, 49 Xilinguole South Road, Hohhot 010020, China*
[3] *Inner Mongolia Guangheyuan Nano High Tech Co., Ltd., 22 Sarula North Road, Ordos 017010, China*
[4] *School of Chemistry and Environmental Science, Inner Mongolia Normal University, 81 Zhaowuda Road, Hohhot 010022, China*
[§] *Juan Liang and Yan Zhang contributed equally to this work.*

Received: 9 April 2026; **Revised:** 10 August 2026; **Accepted:** 10 August 2026

✉ Address correspondence to Xuan Xu, xu.xuan@imu.edu.cn; Peng Jing, pjing@imu.edu.cn; Jun Zhang, cejzhang@imu.edu.cn

Cite this article: *Nano Research*, 2026, 19, 94909100 https://doi.org/10.26599/NR.2026.94909100

ABSTRACT: The high hardness and chemical inertness of SiC hinder its efficient material removal and surface planarization during chemical mechanical polishing (CMP). Although Fenton-like reactions have been explored to promote SiC surface oxidation, conventional physically mixed catalyst-abrasive systems often suffer from poor dispersion and require external fields to enhance the catalytic reaction. The novelty of this work lies in the construction of integrated Cu_xO-CeO_2/Al_2O_3 composite abrasives, in which Cu_xO-CeO_2 Fenton-like catalysts are directly supported on commercial Al_2O_3 abrasives to couple catalytic oxidation and mechanical abrasion without external-field assistance. In SiC polishing, the composite abrasives deliver a material removal rate of 538.45 nm/h and a surface roughness of 0.629 nm over 50 × 50 μm^2, with a damaged layer thickness of 2.3 nm. CeO_2, owing to its low Mohs hardness and low elastic modulus, improves the wetting and frictional properties of the composite abrasives and promotes the formation of active Cu^+ species. The Cu^+ species catalyze the decomposition of H_2O_2 to generate highly oxidative ·OH radicals, which promote SiC surface oxidation and facilitate its subsequent removal by Al_2O_3 abrasives. This synergistic mechanism involving Fenton-like oxidation and mechanical abrasion was investigated by combining transmission electron microscopy and time-of-flight secondary ion mass spectrometry with electron paramagnetic resonance spectroscopy for the identification of reactive radicals.

KEYWORDS: SiC, Al_2O_3, Cu_xO-CeO_2, Fenton-like reaction, chemical mechanical polishing

1 Introduction

With the increasing demand for high-temperature-resistant, radiation-resistant, and high-power electronic devices in modern industries, third-generation semiconductor materials such as silicon carbide (SiC), have become indispensable for strategic applications. [1-3] The application of SiC and diamond in integrated circuit and semiconductor industry requires atomically smooth and defect-free surfaces. [4, 5] However, its high hardness and chemical inertness limit chemical reactions with acids or bases at room temperature, making the precise polishing of SiC a challenging task. [6, 7] Chemical mechanical polishing (CMP), which integrates mechanical abrasion with chemical reactions, widely employs ceria abrasives, enabling atomic-level global planarization. [8-12] However, toxic and corrosive slurries are usually used in conventional CMP, resulting in the high waste treatment costs. [13] For example, strong oxidizing agents such as $KMnO_4$ are generally required to promote surface oxidation of SiC. To address these limitations, novel environmentally friendly CMP processes were developed for diamond, silicon, copper, sapphire, alloy, fused silica, quartz glass and epoxy resin, et al. [14-21] Using the developed green CMP, atomic level surfaces are garnered for the potential use in integrated circuit and semiconductors. [22] These advances have promoted the development of more sustainable CMP processes while reducing the pollution to the environment. [23]

In recent years, the Fenton reaction has garnered significant attention within the CMP field. [24-26] The Fenton reaction typically occurs at a pH of 2.5-4, where Fe^{2+} induces the catalytic decomposition of H_2O_2 to produce ·OH radicals. Under the influence of ·OH, the SiC surface undergoes oxidation reaction to form a softer and more

chemically active SiO_2 layer, thereby enabling efficient CMP process. [27] Lu et al. analyzed the effect of ·OH concentration on the chemical reaction rate on SiC surface. The higher ·OH concentration, the faster chemical reaction rate was achieved on SiC surface. [28] However, the Fenton-CMP system requires operation in a strongly acidic environment (pH < 3), which suffers from low abrasive dispersity that limits the polishing performance.

Similar to Fenton reactions, Fenton-like reactions involve advanced oxidation mechanisms, which produce radicals through the activation of H_2O_2 or other oxidants by transition metal-based catalysts or external energy sources in non-conventional Fe^{2+}/H_2O_2 systems. [29, 30] The promising potential of Fenton-like system presents a new avenue for advancing surface CMP technology for high hardness materials such as SiC. Yuan et al. employed ultraviolet (UV) light to assist the decomposition of H_2O_2 catalyzed by TiO_2 to produce ·OH radicals, thereby enhancing the polishing performance for SiC. A maximum material removal rate (MRR) of 950 nm/h and a minimum surface roughness (Sa) of 0.35 nm was achieved. [31] Deng et al. performed electrochemical mechanical polishing for SiC by anodizing SiC during polishing and an MRR of 3.62 μm/h was achieved. [32] Zhou et al. reported that the polishing slurries containing Pt/C and Fe as catalysts facilitated the production of more ·OH radicals, increasing the MRR to over 120 nm/h for SiC, with a Sa of as low as 0.05 nm. [33] Chen et al. developed a novel polishing slurry composed of Fe, graphene oxide (GO), and Al_2O_3. The slurry achieved a MRR of 700 nm/h and reduced the average Sa to 0.6157 nm due to the enhanced dispersity of Fe with addition of GO. [34] However, these techniques require the use of external field devices (e.g., light, electric fields) or the introduction of expensive materials, which not only increases processing cost but also introduces challenge in the dispersion of both the abrasives and the heterogeneous catalysts in the polishing slurry, thereby affecting polishing performance.

When polishing SiC surface with commercial abrasives (diamond, Al_2O_3, CeO_2, and SiO_2), there are significant limitations regarding the MRR or Sa (Fig. S1 in the Electronic Supplementary Material (ESM)). Diamond is mainly utilized for rough polishing (MRR: 1363.50 nm/h) but cannot directly yield atomically smooth surface (Sa: 4.46 nm). Al_2O_3 abrasives, although providing high MRR (163.51 nm/h), tend to leave microscopic scratches on the polished surface (Sa: 3.31 nm). CeO_2, owing to relatively low Mohs hardness (~ 7), exhibits limited effectiveness in the high-precision planarization of SiC (MRR: 135.74 nm/h, Sa: 0.67 nm). Colloidal SiO_2 typically delivers a low MRR of 98.72 nm/h with a Sa of 0.92 nm. Therefore, the development of novel composite abrasives that can overcome the inherent trade-off between polishing efficiency and precision is of considerable scientific and practical significance.

Herein, this work develops novel composite abrasives by integrating Cu_xO-CeO_2 Fenton-like catalysts with commercial Al_2O_3 abrasives. The introduction of CeO_2 with low Mohs hardness and elastic modulus enhances the wetting and frictional properties of the abrasives, while promoting the formation of Cu^+ active species that catalyze H_2O_2 decomposition into highly oxidative ·OH radicals. The synergistic contribution involving Fenton-like oxidation and mechanical abrasion is elucidated through comprehensive characterizations. The composite abrasives achieve a high MRR of 538.45 nm/h for SiC with a Sa of 0.629 nm, demonstrating their potential for efficient SiC polishing.

2 Results and discussion

2.1 Characterizations of Cu_xO-CeO_2/Al_2O_3 composite abrasives

A simple precipitation-calcination method was employed to synthesize Cu_xO-CeO_2/Al_2O_3 and other abrasives (Fig. S2 and Table S1 in the ESM). The phase composition, the microstructure, and the valence states of the composite abrasives were thoroughly characterized. **Fig. 1(a)** shows the X-ray diffraction (XRD) pattern of Cu_xO-CeO_2/Al_2O_3. The characteristic peaks at 25.60°, 35.19°, 43.40°, and 57.58° correspond to (012), (104), (113), and (116) crystal planes of Al_2O_3 (PDF#97-000-9771), respectively. The four characteristic peaks at 28.50°, 33.08°, 47.48°, and 56.34° correspond to (111), (200), (220), and (311) crystal planes of CeO_2 (PDF#97-002-9046), respectively. The weak peak at 38.75° corresponds to (111) crystal plane of CuO (PDF#97-001-6025). Fig. S3 in the ESM shows XRD patterns of the other three abrasives, Al_2O_3, Cu_xO/Al_2O_3 and CeO_2/Al_2O_3. Only peaks of Al_2O_3 are observed for Al_2O_3 abrasives, while peaks of CuO and CeO_2 can be identified for Cu_xO/Al_2O_3 and CeO_2/Al_2O_3, respectively. These results preliminarily show that Cu and Ce were successfully loaded onto Al_2O_3 particles in the form of oxides.

The microstructure of Cu_xO-CeO_2/Al_2O_3 composite abrasives was further analyzed using scanning electron microscopy (SEM) and transmission electron microscopy (TEM). Fig. S4 in the ESM shows the morphology of the four different samples, revealing that the individual Al_2O_3 particles exhibit irregular polygonal shapes with sharp edges, measuring approximately 200-300 nm in size. Cu_xO/Al_2O_3, CeO_2/Al_2O_3, and Cu_xO-CeO_2/Al_2O_3 composite abrasives prepared by the precipitation-calcination method do not differ greatly from Al_2O_3 in terms of morphology, with only slight irregularities on the particle surface. In addition, the energy dispersive X-ray spectroscopy (EDS) elemental mapping image of Cu_xO-CeO_2/Al_2O_3 composite abrasives also shows that Cu or Ce elements are uniformly distributed on Al_2O_3 surface (Fig. S5 in the ESM).

In the TEM image of Cu_xO-CeO_2/Al_2O_3 composite abrasives (**Fig. 1(b)**), the uniformly distributed nanoparticles (< 10 nm) are observed on the surface of Al_2O_3. High-resolution transmission electron microscopy (HRTEM) image (**Fig. 1(c)**) shows that 0.25 nm, 0.31 nm, and 0.23 nm interplanar spacings correspond to (104) plane of Al_2O_3, (111) plane of CeO_2, and (111) plane of CuO, respectively. The corresponding EDS elemental mapping image (**Fig. 1(d)**) again shows that Cu and Ce elements are uniformly distributed on Al_2O_3 supports. For Cu_xO/Al_2O_3 and CeO_2/Al_2O_3 composite abrasives, except the absence of CeO_2 and Cu_xO, respectively, they show similar microstructure as Cu_xO-CeO_2/Al_2O_3 (Fig. S6 in the ESM). Table S2 in the ESM shows the theoretical and actual contents (wt.%) of Cu and

Ce in the three composite abrasives. The actual content is slightly lower than the theoretical content, which can be attributed to normal loss during the loading procedure.

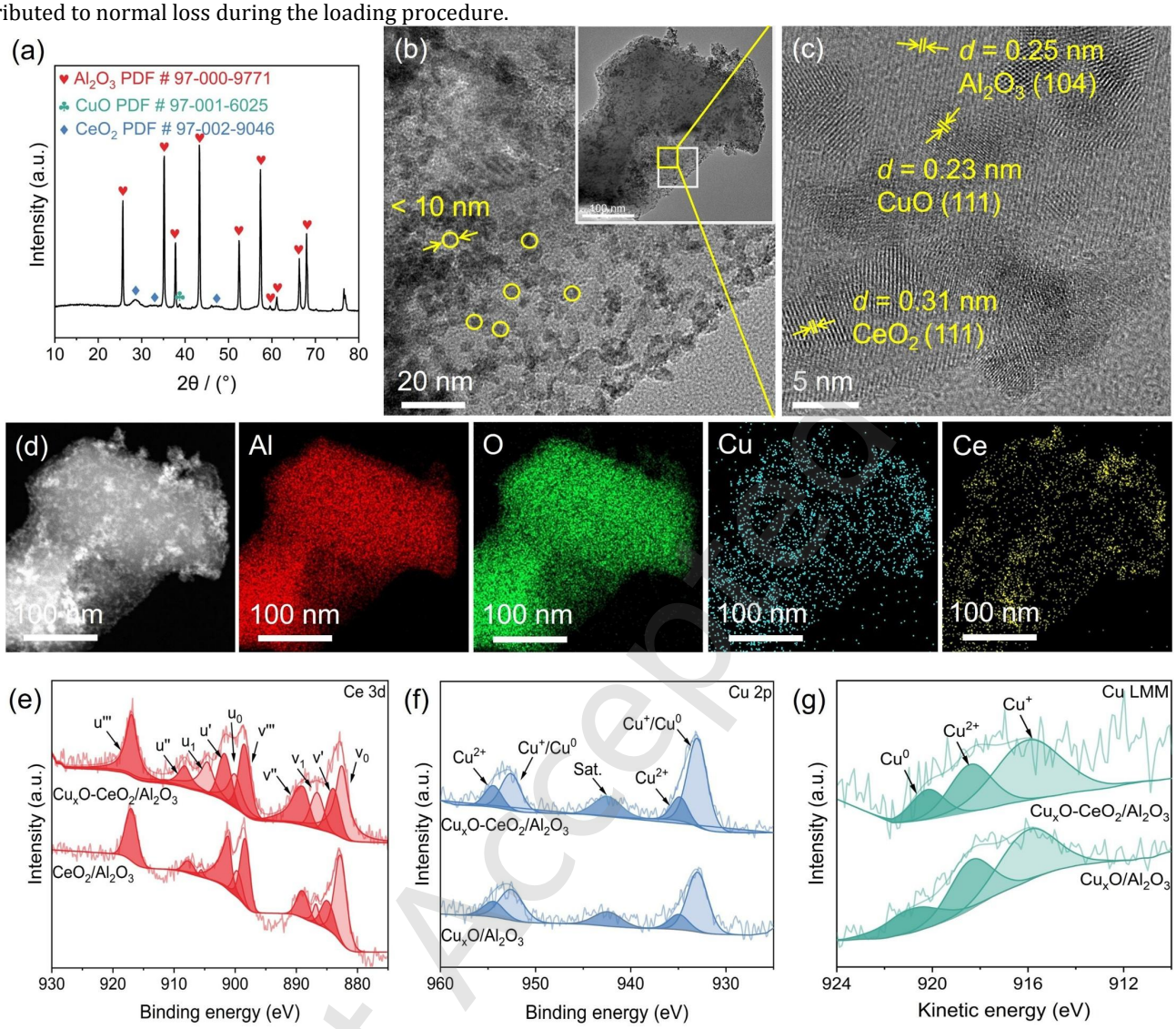

Figure 1. Characterizations of Cu_xO-CeO_2/Al_2O_3 composite abrasives. (a) XRD, (b) TEM, (c) HRTEM and (d) EDS elemental mapping images of Cu_xO-CeO_2/Al_2O_3 composite abrasives. Inset in (b) shows the image at high magnification. (e) Ce 3d XPS of CeO_2/Al_2O_3 and Cu_xO-CeO_2/Al_2O_3 composite abrasives. (f) Cu 2p XPS and (g) Cu LMM Auger spectra of Cu_xO/Al_2O_3 and Cu_xO-CeO_2/Al_2O_3 composite abrasives.

X-ray photoelectron spectroscopy (XPS) was used to characterize the surface valence states of the four abrasives. The presence of Al, O, Cu, and Ce elements is observed in the XPS survey spectra (Fig. S7 in the ESM). Ce 3d XPS spectra (**Fig. 1(e)**) can be fitted into five pairs of peaks, with two sets of peaks (Ce $3d_{3/2}$ and Ce $3d_{5/2}$) typically denoted as u and v, respectively. Among these characteristic peaks, v_0, v_1, u_0, and u_1 correspond to Ce^{3+}, while the remaining characteristic peaks correspond to Ce^{4+}. The results show that both Ce^{3+} and Ce^{4+} valence states coexist in CeO_2/Al_2O_3 and Cu_xO-CeO_2/Al_2O_3composite abrasives. [35] In addition, the Ce^{3+} concentration of Cu_xO-CeO_2/Al_2O_3 was calculated to be 43.07% by semi-quantitative calculation, which is higher than that of CeO_2/Al_2O_3 (37.55%). The reason is due to the doping of Cu^{2+} species in CeO_2 in addition to forming Cu_xO phase. [36] These Ce^{3+} species promotes the strong electronic interactions of $Ce^{3+} + Cu^{2+} \leftrightarrow Ce^{4+} + Cu^{+}$, which favors the formation of Cu^{+}. [37, 38] Compared to Cu_xO/Al_2O_3, the higher intensity of Cu^{+} peak in Cu 2p XPS spectrum (**Fig. 1(f)**) and Cu LMM Auger spectrum (**Fig. 1(g)**) of Cu_xO-CeO_2/Al_2O_3 composite abrasives indicate that there are more Cu^{+} species are formed, consistent with the Ce 3d XPS spectra. [38-40]

2.2 CeO_2-Enhanced catalytic performance of Cu_xO-CeO_2/Al_2O_3 composite abrasives

Because the radicals produced from the Fenton-like reaction show oxidizing property, rhodamine B (RhB) degradation was employed as a model reaction to assess the catalytic performance of various abrasives (**Fig. 2(a),** Fig. S8, Fig. S9(a) and S9(b) in the ESM). The RhB degradation efficiency are consistently higher with the addition of different abrasives containing Cu_xO or CeO_2 compared to that in the absence of abrasives, with the highest degradation reaction rate being observed for Cu_xO-CeO_2/Al_2O_3 composite abrasives (pseudo-first-order reaction rate constant (k): 3.54×10^{-2} min^{-1}) > Cu_xO/Al_2O_3 (k: 0.81×10^{-2} min^{-1})> CeO_2/Al_2O_3 (k: 0.61×10^{-2} min^{-1}), which indicates that Cu_xO is more active than CeO_2 to catalyze the H_2O_2 decomposition, while the reaction is further promoted

when Cu_xO-CeO_2 are combined together.

Fig. 2(b) shows the catalytic performance of Cu_xO-CeO_2/Al_2O_3 composite abrasives with different Cu:Ce molar ratios. As the Cu content increases, the degradation efficiency of RhB initially rises and then declines. This can be attributed

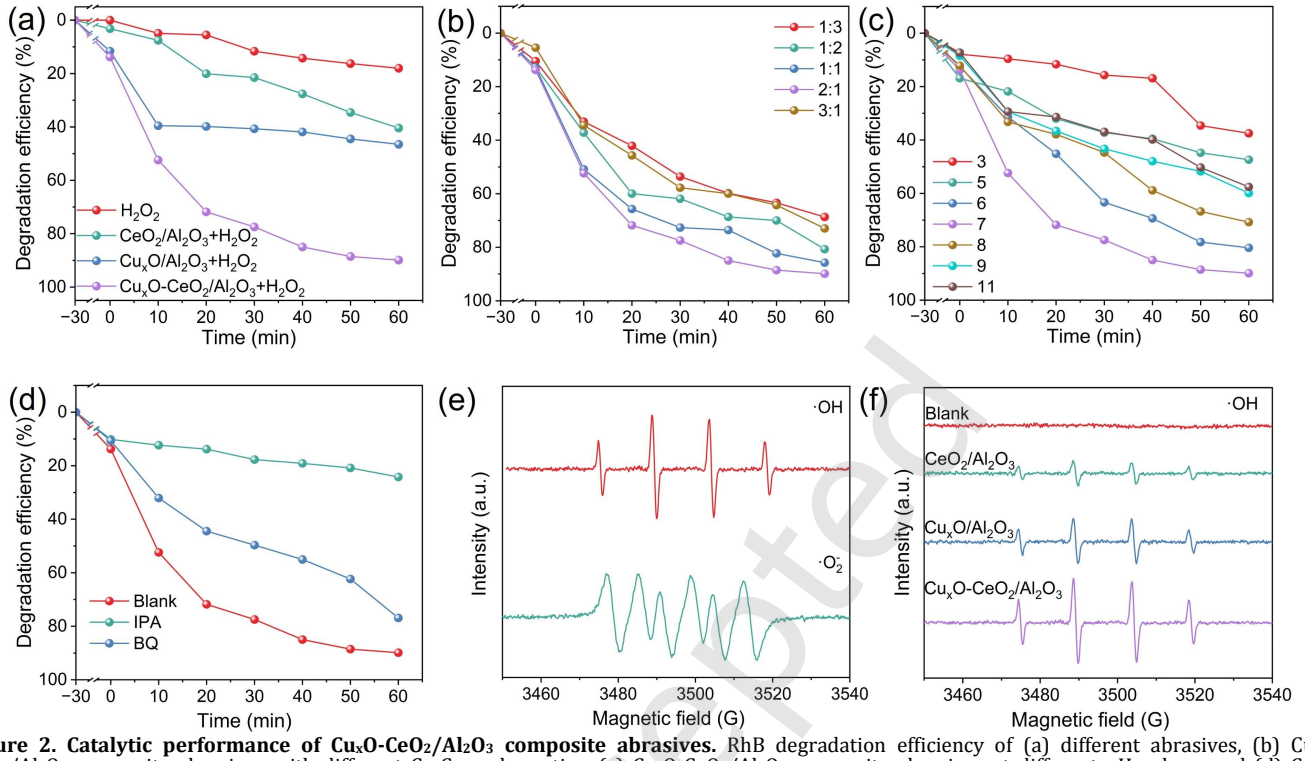

Figure 2. Catalytic performance of Cu_xO-CeO_2/Al_2O_3 composite abrasives. RhB degradation efficiency of (a) different abrasives, (b) Cu_xO-CeO_2/Al_2O_3 composite abrasives with different Cu:Ce molar ratios, (c) Cu_xO-CeO_2/Al_2O_3 composite abrasives at different pH values, and (d) Cu_xO-CeO_2/Al_2O_3 composite abrasives with different scavengers at pH of 7. (e) DMPO-involved EPR spectra of Cu_xO-CeO_2/Al_2O_3 composite abrasives and (f) different abrasives in the presence of H_2O_2.

to insufficient active Cu sites participating the H_2O_2 decomposition at low Cu:Ce molar ratio. Further increasing the Cu:Ce molar ratio to 3:1 leads to catalyst agglomeration, thereby decreasing the catalytic activity. [41, 42] The highest degradation reaction rate (k: 3.54×10^{-2} min^{-1}) is observed when the Cu:Ce molar ratio is 2:1 (Fig. S9(c) and S9(d) in the ESM). Therefore, the Cu:Ce molar ratio was fixed at 2:1 in the following experiments. Meanwhile, the degradation reaction rates of RhB are highly dependent on the pH values. [43] At pH of 7, Cu_xO-CeO_2/Al_2O_3 composite abrasives show the highest degradation reaction rate (**Fig. 2(c),** Fig. S9(e) and S9(f) in the ESM). The production of HO_2^- at acidic condition and O_2 at alkaline condition by H_2O_2 decomposition are not favorable for RhB degradation in aqueous solution. [44]

Radical scavenge experiments were performed to further elucidate the type of radicals involved in the degradation of RhB. A scavenger is a reagent that helps identify and confirm the dominant active species by selectively inhibiting specific radicals. [45] As shown in **Fig. 2(d),** Fig. S9(g) and S9(h) in the ESM, when benzoquinone ($C_6H_4O_2$, BQ, $·O_2^-$ scavenger) was added, the degradation reaction rate (k) for RhB decreased from 3.54×10^{-2} min^{-1} to 1.95×10^{-2} min^{-1}. In contrast, the addition of isopropanol (C_3H_8O, IPA, ·OH scavenger) resulted in a significant drop of k value to only 0.28×10^{-2} min^{-1}. The addition of IPA notably inhibited the degradation of RhB, which indicates that ·OH radicals plays a dominant role in Fenton-like reaction and is the primary active species.

Electron paramagnetic resonance (EPR) spectroscopy was employed to further identify the type of produced radicals in the presence of H_2O_2 and Cu_xO-CeO_2/Al_2O_3 composite abrasives with DMPO ($C_6H_{11}NO$) as the trapping reagent. [46] As shown in **Fig. 2(e)**, two signals corresponding to ·OH and $·O_2^-$ are detected, which is consistent with the results presented in **Fig. 2(d)**. **Fig. 2(f)** shows the EPR spectra of different abrasives in the presence of H_2O_2. It can be observed that the ·OH signal is scarcely detectable in the absence of abrasives, as the content of ·OH produced by the self-decomposition of H_2O_2 is minimal. However, when the abrasives are introduced, the ·OH signal is significantly enhanced, with Cu_xO-CeO_2/Al_2O_3 composite abrasives showing the highest signal intensity. These results suggest that the presence of Cu_xO-CeO_2 can efficiently catalyze the H_2O_2 decomposition to produce more ·OH radicals.

2.3 CeO_2-Enhanced polishing performance of Cu_xO-CeO_2/Al_2O_3 composite abrasives

The polishing tests were performed on SiC by UNIPOL-1200S CMP equipment (Fig. S10 in the ESM). The as-prepared abrasives exhibit a uniform appearance, while the corresponding polishing slurry remains well dispersed without obvious aggregation state. The polishing performance (MRR and Sa) for SiC with different abrasives was evaluated (**Fig. 3(a) and 3(b),** Fig. S11-S13 in the ESM) by preparing polishing slurry. When the polishing slurry contained only Al_2O_3 abrasives without the addition of oxidizing H_2O_2, Al_2O_3 abrasives show very poor polishing performance for SiC with a MRR of 131.44 nm/h and a Sa of

7.596 nm. This suggests that the efficiency of mechanical polishing without the assistance of chemical reaction is limited. Upon introducing H_2O_2 as an oxidant, the chemical mechanical polishing based on the synergistic effect of chemical oxidation and mechanical polishing achieves a MRR increased to 163.74 nm/h and a Sa of 3.143 nm. During CMP process, SiC surface is subjected to brief high temperature and friction under specific downward pressure and rotational speed. These conditions also facilitate the generation of ·OH radicals, thereby accelerating the oxidation of SiC surface. The formation of a surface oxidation layer on SiC by oxidant can improve the efficiency of mechanical polishing. Meanwhile, the chemical oxidation initially softens the surface layer, mitigating mechanical damage of SiC surface. [47, 48]

When the composite abrasives (CeO_2/Al_2O_3 and Cu_xO/Al_2O_3) and H_2O_2 were employed, further improved polishing efficiencies are obtained. CeO_2/Al_2O_3 composite abrasives show a MRR of 253.81 nm/h and a Sa of 1.707 nm while Cu_xO/ Al_2O_3 composite abrasives show a MRR of 274.38 nm/h and a Sa of 1.301 nm. For Cu_xO-CeO_2/Al_2O_3 composite abrasives, the highest MRR of 538.45 nm/h and the lowest Sa of 0.629 nm are achieved, which is comparable to the recently reported abrasives (Table S3 in the ESM). The performance of Cu_xO-CeO_2/Al_2O_3 composite abrasives was also systematically compared with several emerging CMP strategies, including catalysis-assisted CMP, UV-assisted CMP, and mixed-abrasive CMP. The Cu_xO-CeO_2 composite abrasives integrate Fenton-like catalytic sites with Al_2O_3 abrasives, enabling efficient chemical-mechanical polishing of SiC under mild conditions without the need for external fields or strong oxidizing agents. These results suggest that by introducing the Fenton-like catalysts (Cu_xO or CeO_2) for H_2O_2 decomposition, a higher degree of surface oxidation of SiC can be achieved by generating more ·OH radicals as discussed below. This enables synergistic effect of chemical oxidation and mechanical abrasion, thus leading to significantly improved polishing efficiency by CMP. Meanwhile, CeO_2 promotes the formation of active Cu^+ species, therefore enabling the highest polishing performance of Cu_xO-CeO_2/Al_2O_3 composite abrasives, which is consistent with its highest catalytic performance as discussed in section 2.2. [37, 38]

Relying solely on roughness values across the entire surface may not fully capture the spatial variations in surface topography, as these values can be influenced by random peaks or valleys. [49, 50] Therefore, to further characterize the polishing performance of different abrasives, two lines were collected in 2D surface images of polished SiC for height difference measurements (Fig. S12(a) in the ESM). As shown in Fig. S13 in the ESM, the curve with Cu_xO-CeO_2/Al_2O_3 (Fig. S13(f) in the ESM) exhibits the mildest fluctuations, again showing the enhanced polishing performance of Cu_xO-CeO_2/Al_2O_3 composite abrasives.

Raman spectroscopy was employed to analyze the SiC surface before and after polishing with Cu_xO-CeO_2/Al_2O_3 slurry. Raman test points were marked by circles in Fig. S14 in the ESM. Raman spectrum (**Fig. 3(c)**) exhibits two prominent characteristic peaks, E_2 (TO) and A_1 (LO), corresponding to the transverse optical (TO) and longitudinal optical (LO) modes of SiC, respectively. The E_2 (TO) peak is located at approximately 790 cm^{-1}, representing the high-frequency phonon mode, while the A_1 (LO) peak, situated near 960 cm^{-1}, corresponds to the low-frequency longitudinal phonon mode. [51, 52] Mechanical processing or pretreatment can induce lattice distortion, microcracks, or defects on the surface, thereby enhancing phonon scattering effects, which broadens the peak and reduces peak intensity in Raman spectrum. Additionally, residual stress in the damaged layer can further broaden the energy distribution of the phonon mode. The characteristic SiC peaks after polishing become strong, signifying a more regular lattice structure and improved surface quality. A broad peak in the range of 500-600 cm^{-1} is also observed in the spectrum prior to polishing, which is attributed to the surface damaged layer. [53] After polishing, this broad peak at 500-600 cm^{-1} significantly weakened, indicating the removal of defects, microcracks, or amorphous regions on the surface.

Compared with the rough and opaque unpolished SiC surface, the SiC surface after polishing with Cu_xO-CeO_2/Al_2O_3 composite abrasives exhibits a mirror-like finish (Fig. S15(a, b) in the ESM). The optical morphology (Fig. S15(c, d) in the ESM) and SEM images (Fig. S15(e, f) in the ESM) of SiC surface further show that prior to polishing, the surface exhibits numerous scratches and irregular pits, whereas after polishing, the surface becomes smooth without scratches and grinding pits. The thickness of the damaged layer for SiC after polishing with Cu_xO-CeO_2/Al_2O_3 composite abrasives was characterized by cross-sectional TEM (Fig. S15(g, h) in the ESM and **Fig. 3(d, e)**). The surface quality of the polished SiC has been significantly improved, and the thickness of the subsurface damaged layer is measured to be approximately 2.3 nm, demonstrating the excellent polishing performance of the composite abrasives.

The MRR and the Sa of SiC after polishing with Cu_xO-CeO_2/Al_2O_3 composite abrasives with different Cu:Ce molar ratios are shown in **Fig. 3(f)** and Fig. S16 in the ESM. The results indicate that as the Cu:Ce ratio increases, the MRR initially increases and then decreases. At the Cu:Ce ratio of 2:1, the MRR reaches a peak value of 533.89 nm/h. However, when the Cu:Ce ratio further increases to 3:1, the MRR decreases to 423.93 nm/h. In contrast, Sa follows an opposite trend, reaching its minimum value of 0.660 nm at the Cu:Ce ratio of 2:1. These results is same as the trend observed in catalytic performance (**Fig. 2(b)**).

Polishing experiments were also conducted for SiC using Cu_xO-CeO_2/Al_2O_3 polishing slurry with different pH values (**Fig. 3(g)** and Fig. S17 in the ESM). As the pH value of the polishing slurry increases from 5 to 9, both the MRR and the Sa show notable non-linear trends. The highest MRR of 531.45 nm/h and the lowest Sa of 0.639 nm are obtained at neutral pH of 7, which is consistent with the trend in catalytic performance at different pH values (**Fig. 2(c)**). The production of ·OH radicals at pH of 7 accelerates the formation of a soft oxide layer that can be removed by mechanical polishing on SiC surface, thereby keeping a low Sa value. The alkaline polishing slurry may induce excessive hydration reaction on SiC surface, leading to a loose structure prone to generating flaking defects during

mechanical polishing. [54]

In addition, the isoelectric point (IEP) of SiC and Cu_xO-CeO_2/Al_2O_3 composite abrasives are approximately 3.3 and 8.2, respectively (Fig. S18 in the ESM). When the pH lies between 3.3 and 8.2, SiC workpiece and Cu_xO-CeO_2/Al_2O_3 composite abrasives possess opposite charges, leading to strong electrostatic attraction between them, which enhances the contact and friction between the two materials. [55]

Furthermore, the influence of abrasive concentrations (**Fig. 3(h),** Fig. S19 and S20 in the ESM) and H_2O_2 concentrations

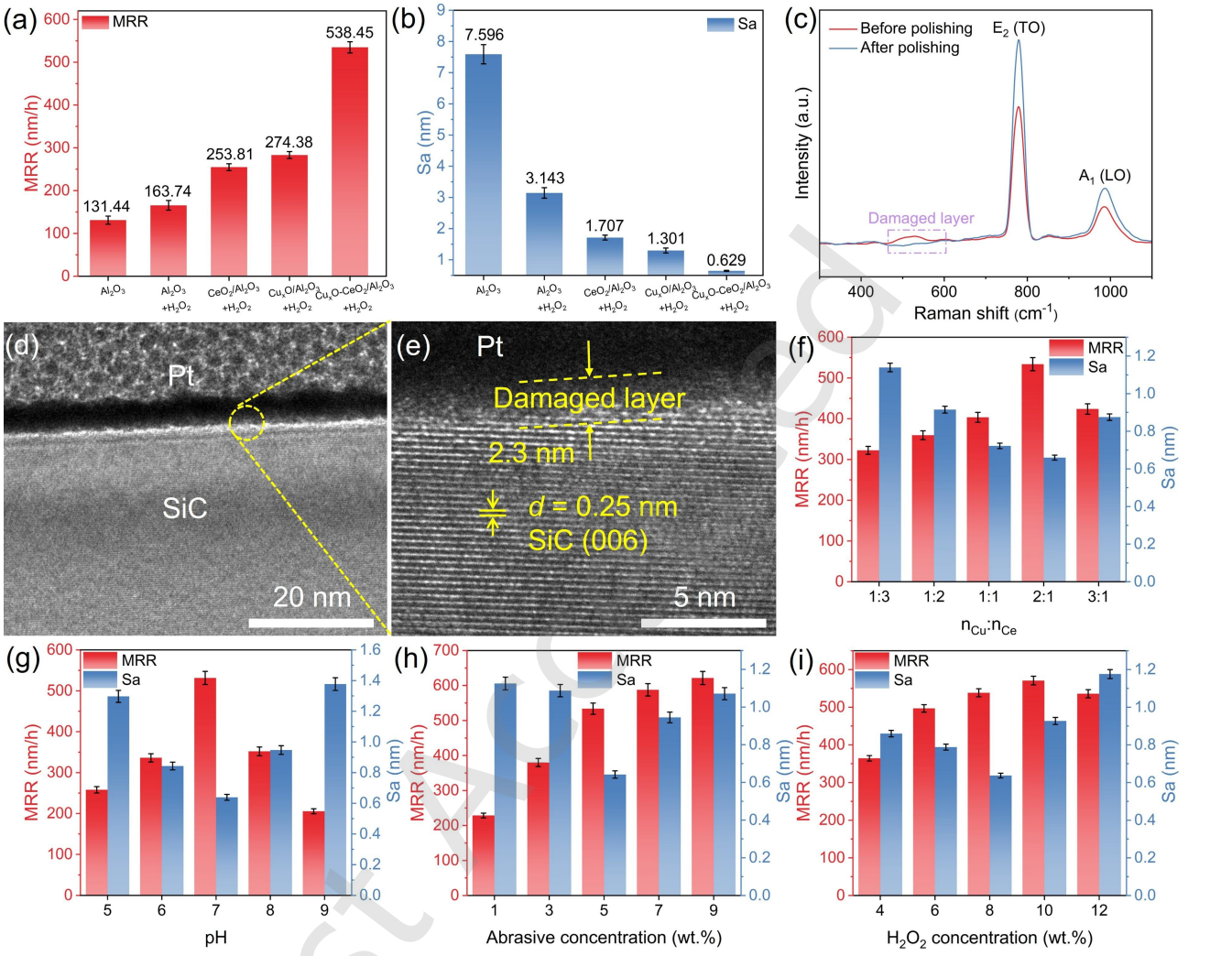

Figure 3. Polishing performance of Cu_xO-CeO_2/Al_2O_3 composite abrasives. (a) MRR and (b) Sa of SiC after polishing with different abrasives. (c) Raman spectra of SiC surface before and after polishing with Cu_xO-CeO_2/Al_2O_3 composite abrasives. Cross-sectional (d) TEM and (e) HRTEM images of SiC after polishing with Cu_xO-CeO_2/Al_2O_3 composite abrasives. (f) MRR and Sa for SiC after polishing with Cu_xO-CeO_2/Al_2O_3 composite abrasives with different Cu:Ce molar ratios. MRR and Sa of SiC polished with Cu_xO-CeO_2/Al_2O_3 polishing slurries with different (g) pH values, (h) abrasive concentrations, and (i) H_2O_2 concentrations.

(**Fig. 3(i),** Fig. S21 and S22 in the ESM) on the polishing performance of Cu_xO-CeO_2/Al_2O_3 composite abrasives were studied. The MRR increases continuously from 228.54 nm/h at 1 wt.% to 621.47 nm/h at 9 wt.% with increasing abrasive concentrations (**Fig. 3(h)**). Conversely, the Sa exhibits a non-monotonic trend, reaching a minimum value of 0.642 nm at 5 wt.%. At low abrasive concentrations (1-5 wt.%), the polishing slurry shows low viscosity (Fig. S19 in the ESM), enabling good flowability and uniform abrasive dispersity. [56, 57] However, insufficient abrasives result in low MRR values and the inadequately removal of mechanical damages contributes to higher Sa values. In contrast, at higher abrasive

concentrations (7-9 wt.%), increased viscosity promotes abrasive agglomeration. While these larger agglomerates enhance the MRR value, they concurrently induce pronounced surface scratches, thereby increasing the Sa value.

For H_2O_2 concentration, the change in the oxidation reduction potential (ORP) of polishing slurry with different H_2O_2 concentrations were measured (Fig. S21(a) in the ESM). Higher H_2O_2 concentrations correspond to higher initial ORP values (12 wt.% > 10 wt.% > 8 wt.%), signifying an increased oxidation capacity. However, as the time extends, the ORP value decreases gradually. Notably, the ORP decay rate is faster for polishing slurries with higher H_2O_2 concentrations, such as 12 wt.%, likely due to the scavenging effect of excess H_2O_2 on ·OH. [58, 59] EPR measurement at varying H_2O_2 concentrations was carried out to study the scavenging effect of excess H_2O_2 on ·OH. As shown in Fig. S21(b) in the ESM, at the initial stage, the slurries containing higher concentrations of H_2O_2 show markedly intensified ·OH

signals. After 40 min, the ·OH signals of the slurries with 10 wt.% and 12 wt.% H_2O_2 attenuated to levels that were even lower than those for the slurry with 8 wt.% H_2O_2 (Fig. S21(c) in the ESM). This trend is consistent with the ORP results and further confirms the scavenging of ·OH by excess H_2O_2. **Fig. 3(i)** shows the MRR and the Sa of SiC after polishing with slurries with different H_2O_2 concentrations. As the H_2O_2 concentration increases from 4 wt.% to 12 wt.%, the MRR first increases and then decreases, reaching a peak value of 570.76 nm/h at 10 wt.%, the Sa follows an opposite trend, initially decreasing and then increasing with a minimum value of 0.637 nm being observed at 8 wt.%. Thus, to balance the MRR value and the Sa value, the H_2O_2 concentration is fixed at 8 wt.%.

Experiments have been also carried out to evaluate the reusability and the storage stability of the composite abrasives (Fig. S23 in the ESM). The Cu_xO-CeO_2/Al_2O_3 polishing slurry were reused for 10 consecutive polishing cycles. As shown in Fig. S23(a) in the ESM, the MRR for SiC decreases gradually as the cycle number increases and drops sharply after 8 cycles. After 10 cycles, the MRR is approximately 360 nm/h. Meanwhile, the Sa remains essentially unchanged during the 10 cycles, showing it excellent reusability. Furthermore, a 14-day storage stability test (Fig. S23(b) in the ESM) shows that the Cu_xO-CeO_2/Al_2O_3 polishing slurry exhibits an approximately 40% decrease in MRR, which may be attributed to the gradual decomposition of H_2O_2 during storage due to the absence of a stabilizer in the slurry. Therefore, this polishing slurry is recommended to be used within 1-2 weeks.

2.4 Polishing mechanisms of Cu_xO-CeO_2/Al_2O_3 composite abrasives

The CMP process is influenced by both chemical oxidation and mechanical polishing between the abrasives and the SiC surface. For the mechanical polishing, the contact angle between the aqueous polishing slurry and the workpiece affects the degree of contact between the abrasives and the SiC surface. Under simulated CMP condition, the contact angles of polishing slurries containing various abrasives on SiC surface are shown in **Fig. 4(a)**. The contact angle of deionized water on SiC is 57.32°. The contact angle increases with the addition of Al_2O_3 (66.65°) polishing slurry, likely due to the aggregation of abrasives which forms local hydrophobic areas. This hinders the uniform contact between the abrasives and the Al_2O_3 surface. The contact angles for CeO_2/Al_2O_3 (51.72°), Cu_xO/Al_2O_3 (55.66°), and Cu_xO-CeO_2/Al_2O_3 (46.48°) polishing slurries on SiC are all lower than that of Al_2O_3 polishing slurry, with Cu_xO-CeO_2/Al_2O_3 polishing slurry exhibiting the smallest contact angle. The polishing slurry composed of Cu_xO-CeO_2/Al_2O_3 composite abrasives demonstrates strong wettability for SiC surface, which can be attributed to the formation of hydroxyl groups and oxygen vacancies on the abrasive surface. [37] This also contribute to the improved polishing performance of Cu_xO-CeO_2/Al_2O_3 composite abrasives. Furthermore, CeO_2, with relatively low Mohs hardness of ~ 7, increases the contact area between the abrasives and the hard SiC by microstructure deformation. [60]

The friction behavior of abrasives on SiC is another factor that influence the mechanical polishing efficiency. Therefore, the dynamic friction coefficient change of different abrasives were measured (**Fig. 4(b),** Fig. S24 in the ESM). The friction coefficient of Al_2O_3 polishing slurry on SiC surface increases rapidly during the first 50 s. As the friction time extended, the coefficient gradually decreases and stabilizes at 0.34 after 600 s. This behavior indicates that Al_2O_3 abrasives undergo significant abrasion during the initial contact with SiC surface, resulting in strong collisions and friction. The friction coefficient reduces as the sharp edges of Al_2O_3 abrasives are removed. In contrast, the friction coefficient of Cu_xO-CeO_2/Al_2O_3 polishing slurry on SiC surface remains low during the first 50 s, and subsequently increases to a relatively stable value of 0.26 after 600 s. According to the principle of elastic-plastic deformation, the contact stress between Cu_xO-CeO_2/Al_2O_3 composite abrasives and the SiC is relatively low because of the existence of CeO_2 with lower elastic modulus, which are more effective in achieving better planarization while minimizing surface damage on SiC. [61-63] In a typical CMP process, MRR generally increases with higher friction coefficient between the polishing slurry and SiC. However, the MRR is 163.74 nm/h with a Sa of 3.143 nm when using Al_2O_3 polishing slurry. In comparison, the Cu_xO-CeO_2/Al_2O_3 polishing slurry with lower friction coefficient achieves a higher MRR of 538.45 nm/h and a Sa of 0.629 nm. This suggests that the mechanical polishing is not the main factor that influence the CMP process for SiC.

To study the chemical oxidation process during CMP, SiC was polished with both Al_2O_3 and Cu_xO-CeO_2/Al_2O_3 polishing slurries for 20 min. Afterward, the polished SiC was characterized using SEM and time-of-flight secondary ion mass spectrometry (TOF-SIMS). Upon immersion in Al_2O_3 polishing slurry, no significant change is observed on SiC surface (Fig. S25(a) in the ESM). In contrast, numerous clearly visible white circular spots with oxidized traces are observed on SiC surface after immersed in Cu_xO-CeO_2/Al_2O_3 polishing slurry (Fig. S25(b) in the ESM), showing a higher degree of oxidation. [64]

In the TOF-SIMS analysis, the O^- fragments with a mass-to-charge ratio of 16 are derived from the surface oxide layer or the dissociation of adsorbed oxygen. The signal intensity of these O^- fragments is positively correlated with the thickness of the oxide layer, as thicker oxide layers provide more oxygen atoms available for ionization. [65] **Fig. 4(c) and 4(d)** show the distribution of O^- fragments on SiC surface after immersed in Al_2O_3 and Cu_xO-CeO_2/Al_2O_3 polishing slurries. The SiC surface treated with Cu_xO-CeO_2/Al_2O_3 polishing slurry shows a more uniform and intense oxide layer signals (blue spots), again showing a higher degree of oxidation as more ·OH radicals are produced from H_2O_2 with Cu_xO-CeO_2/Al_2O_3 composite abrasives.

XPS was also employed to examine the changes in SiC surface before and after polishing with Cu_xO-CeO_2/Al_2O_3 composite abrasives (Fig. S26 in the ESM). [37, 60] Prior to CMP, peaks at 288.16 eV, 286.18 eV, 285.08 eV, 284.50 eV, 283.58 eV, and 282.18 eV in C 1s XPS spectra correspond to C=O, C-O, $Si_4C_4O_4$, C-C, $Si_4C_{4-x}O_2$, and SiC, respectively. After polishing, the peak intensity of C=O, C-O, and $Si_4C_4O_4$ increased. Moreover, from Si 2p XPS spectra, peaks at 101.80

eV, 101.28 eV, and 100.82 eV correspond to SiO_xC_y, Si-C-O, and SiC, respectively. After polishing, a decrease of the peak intensity for SiC is observed, while the peak intensity of SiO_xC_y and Si-C-O increased, suggesting a notable oxidation of SiC surface. Significantly, a peak at 103.12 eV, attributed to SiO_2, appeared, which indicates the oxidation or hydrolysis of part of SiC to carbon-free silicon oxide.

TEM was employed to investigate the polishing and removal mechanisms for SiC by Cu_xO-CeO_2/Al_2O_3 composite abrasives. Fig. S27(a) and S27(b) in the ESM show energy-dispersive X-ray spectroscopy (EDS) elemental mapping images of debris after polishing for SiC with Al_2O_3 abrasives. Region 1 exhibits prominent signals of Al and O, while region 2 shows dominant signals of C and Si. The line scan profile in Fig. S27(c) in the ESM further confirms that region 2 is

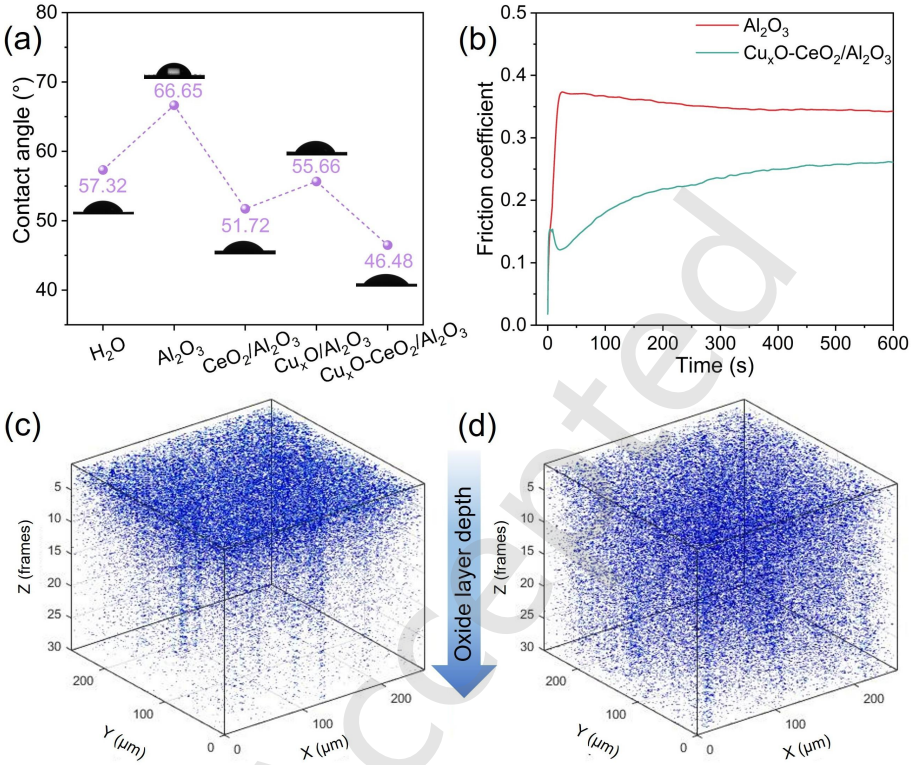

Figure 4. Polishing mechanisms of Cu_xO-CeO_2/Al_2O_3 composite abrasives. (a) The contact angles of different polishing slurries on SiC surface. (b) The dynamic friction coefficient between different polishing slurries and SiC surface. 3D TOF-SIMS images of O^- fragments on SiC surface after polishing with (c) Al_2O_3 and (d) Cu_xO-CeO_2/Al_2O_3 composite abrasives.

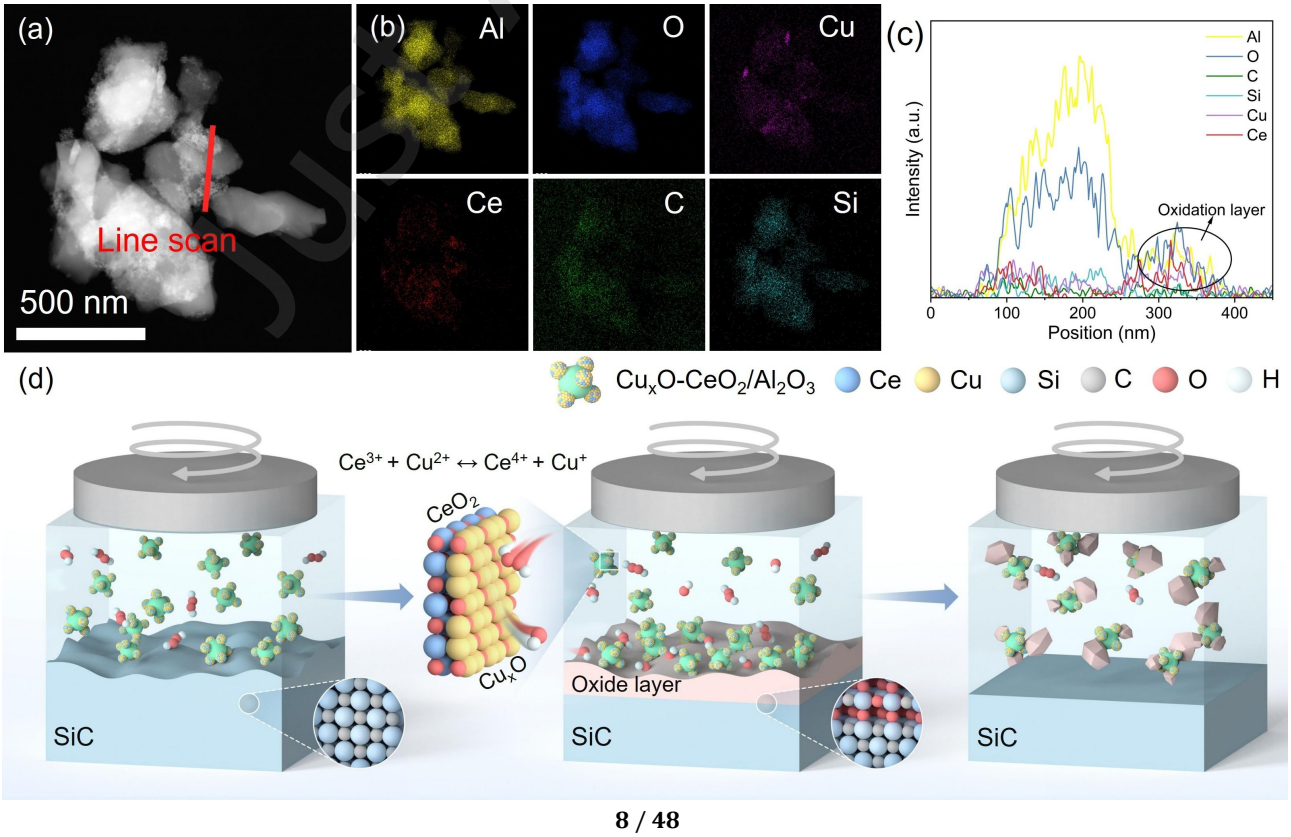

Figure 5. Polishing mechanisms of Cu_xO-CeO_2/Al_2O_3 composite abrasives. (a) TEM image, EDS elemental (b) mapping images and (c) line-scanning profile of SiC debris after polishing with Cu_xO-CeO_2/Al_2O_3 composite abrasives. (d) Schematic diagram of CMP for SiC with Cu_xO-CeO_2/Al_2O_3 composite abrasives.

primarily composed of SiC. This suggests that, after polishing with Al_2O_3 abrasives, the dominant component in the debris is SiC rather than oxidized SiC, and the removal of SiC occurs through brittle fracture induced by the mechanical polishing of Al_2O_3 abrasives. **Fig. 5(a) and 5(b)** show EDS elemental mapping images of debris after polishing for SiC with Cu_xO-CeO_2/Al_2O_3 composite abrasives. Cu_xO and CeO_2 nanoparticles remain supported on Al_2O_3 surface, indicating the good structural stability of composite abrasives. The line scan profile in **Fig. 5(c)** reveals an increase in the signal intensity of Si and O, suggesting that the substance attached to Cu_xO-CeO_2/Al_2O_3 composite abrasives is likely Si-C-O as a result of SiC surface oxidation. This is consistent with the XPS analysis. Therefore, it can be concluded that, unlike the solely mechanical removal mechanism of Al_2O_3 abrasives, the polishing process with Cu_xO-CeO_2/Al_2O_3 composite abrasives is a combination of both chemical oxidation and mechanical abrasion, where the SiC-based oxides rather than SiC are removed.

Based on the above analysis, the CMP mechanism of Cu_xO-CeO_2/Al_2O_3 composite abrasives for SiC is proposed (**Fig. 5(d)**, Fig. S28 in the ESM). CeO_2 promotes the formation of Cu^+ active sites through $Ce^{3+} + Cu^{2+} \leftrightarrow Ce^{4+} + Cu^+$, which catalyze the Fenton-like decomposition of H_2O_2 into highly oxidative ·OH radicals. The generated radicals oxidize the SiC surface, forming a fragile oxide layer that is subsequently removed by abrasive-induced mechanical action. The synergistic chemical-mechanical interaction enables high-efficiency polishing and produces an ultra-smooth SiC surface.

3 Conclusions

A simple precipitation-calcination method was used to prepare novel Cu_xO-CeO_2/Al_2O_3 composite abrasives. The Cu_xO-CeO_2 catalyst for Fenton-like H_2O_2 decomposition facilitates the production of highly oxidative ·OH radicals, which effectively oxidizes the SiC surface to form a soft oxidation layer. This accelerates the mechanical polishing efficiency of Al_2O_3 abrasives. Additionally, the enhanced wettability and the low dynamic friction coefficient of Cu_xO-CeO_2/Al_2O_3 polishing slurry increase the contact area while minimize the surface damage of SiC. Cu_xO-CeO_2/Al_2O_3 composite abrasives achieve a MRR of 538.45 nm/h and a surface roughness of 0.629 nm for SiC through CMP. This work extends the application of CeO_2 in polishing from conventional Si-based substrates to high-hardness materials.

Electronic Supplementary Material: Supplementary material (experimental details, additional characterizations including SEM images, XRD patterns, XPS spectra, HRTEM images, EPR spectra, RhB degradation efficiency, and 3D surface images of SiC after polishing et al.) is available in the online version of this article at https://doi.org/10.26599/NR.2026.94909100.

Data availability

All data needed to support the conclusions in the paper are presented in the manuscript and the Electronic Supplementary Material. Additional data related to this paper may be requested from the corresponding author upon request.

Acknowledgements

This work was supported by the National Natural Science Foundation of China (22361033), the Natural Science Foundation of Inner Mongolia Autonomous Region of China (2024QN02027), the Program of Higher-Level Talents of IMU, the "Grassland Leading Talent" Program of Inner Mongolia, the Inner Mongolia Autonomous Region 2022 Leading Talent Team of Science and Technology (2022LJRC0008).

Declaration of competing interest

All the contributing authors report no conflict of interests in this work.

Author contribution statement

Juan Liang: Writing - original draft, Methodology, Data curation, Conceptualization. Yan Zhang: Writing - original draft, Software, Methodology, Data curation. Zhaokang Li: Methodology. Peng Lv: Software. Wenhao Qi: Software. Hong Feng: Methodology. Xuan Xu: Conceptualization. Baocang Liu: Methodology. Tao Bai: Methodology. Peng Jing: Writing - review & editing, Funding acquisition, Data curation, Conceptualization. Jun Zhang: Writing - review & editing, Funding acquisition, Data curation, Supervision. All the authors have approved the final manuscript.

Use of AI statement

None

References

[1] Matsunami, H. Fundamental research on semiconductor SiC and its applications to power electronics. *Proc. Jpn. Acad. Ser. B.* **2020**, 96, 235-254.

[2] Xu, N.; Zhang, G. S.; Zhang, J.; Gao, Z. H.; Lin, Y.; Huo, Y.; Gao, K. L.; Wang, Y. S. Research progress of CeO_2 based polishing slurry in SiC CMP. *J. Mater. Sci.* **2025**, 60, 21786-21805.

[3] Jiang, K. R.; Zhang, P. L.; Song, S. J.; Sun, T. Z.; Chen, Y.; Shi, H. C.; Yan, H.; Lu, Q. H.; Chen, G. L. A review of ultra-short pulse laser micromachining of wide bandgap semiconductor materials: SiC and GaN. *Mater. Sci. Semicond. Proc.* **2024**, 180, 108559-108579.

[4] Zhao, F.; Zhang, Z. Y.; Deng, X. Q.; Feng, J. Y.; Zhou, H. X.; Liu, Z. S.; Meng, F. N.; Shi, C.J. Atomic surface achieved through a novel cross-scale model from macroscale to nanoscale. *Nanoscale.* **2024**, 16, 2318-2336.

[5] Yu, Z. B.; Zhang, Z. Y.; Zhao, F.; Hu, J. J.; Zhong, S. C.; Ren, Z. Y. Wang, X. R.; Dai, G. Y.; Weng, Q. Review on advanced atomic-level polishing for single crystal diamond. *Surf. Interfaces.* **2025**, 72, 107443-107484.

[6] Chen, Z. J.; Zhan, S. D.; Zhao, Y. H. Electrochemical jet-assisted precision grinding of single-crystal SiC using soft abrasive wheel. *Int. J. Mech. Sci.* **2021**, 195, 106239-106251.

[7] Hu, Y.; Shi, D.; Hu, Y.; Zhao, H. W.; Sun, X. D.; Wang, M. S. Experimental investigation on the ultrasonically assisted single-sided lapping of monocrystalline SiC substrate. *J. Manuf. Process.* **2019**, 44, 299-308.

[8] Zhao, F.; Zhang, Z. Y.; Zhou, H. X.; Feng, J. Y.; Deng, X. Q.; Liu, Z. S.; Meng, F. N.; Shi, C. J. Novel full-scale model verified by atomic surface and developed composite microfiber and slurry polishing system. *Compos. Part B Eng.* **2024**, 283, 111598-111613.

[9] Li, Q. Y.; Zhang, Z. Y.; Wang, Z. Y.; Zhou, H. X.; Zhao, F., Wei, T. L.; Cui, X. X.; Wu, J. F.; Liu, Z. H. Atomic level surface on aluminum alloy produced by novel environmentally-friendly photocatalytic chemical mechanical polishing with high material removal rate using hybrid ceria nanoabrasives. *Tribol. Int.* **2026**, 221, 112080-112092.

[10] Dong, L. G.; Zhang, Z. Y.; Zhao, F.; Li, Q. Y.; Zhou, H. X.; Yang, X. F.; Liu, X. Q.; Guo, J. D.; Zheng, X. Atomic surface on a Ni alloy produced by novel green chemical mechanical polishing. *Tribol. Int.* **2025**, 211, 110902.

[11] Cui, X. X.; Zhang, Z. Y.; Yu, S. Q.; Chen, X.; Shi, C. J.; Zhou, H. X.; Meng, F. N.; Yu, J. X.; Wen, W. Unprecedented atomic surface of silicon induced by environmentally friendly chemical mechanical polishing. *Nanoscale.* **2023**, 15, 9304-9314.

[12] Zhang, Z. Y.; Cui, J. F.; Zhang, J. B.; Liu, D. D.; Yu, Z. J.; Guo, D. M. Environment friendly chemical mechanical polishing of copper. *Appl. Surf. Sci.* **2019**, 467-468, 5-11.

[13] Dong, L. G.; Zhang, Z. Y.; Zhao, F.; Yu, Z. B.; Li, Y.; Wang, J.; Du, W. H.; Tao, C.; Zhang, X. B. Atomic level surface of nickel superalloy induced by novel chemical mechanical polishing and its material removal mechanism elucidated by nanoscratching through molecular dynamics simulations. *Mater. Today Sustain.* **2026**, 35, 101396-101409.

[14] Yu, Z. B.; Jia, Z. H.; Liu, W.; Zhang, Z. Y.; Zhao, F.; Fan, C.; Zhang, H. S.; Lyv, Y. Q.; Liu, D. D. Facet-dependent oxidative fabrication of diamond determined by operando scanning electron microscopy. *Nano Lett.* **2025**, 25, 5391-5397.

[15] Wang, D.; Xie, W. X.; Zhang, Z. Y.; Wang, J. M.; Shi, C. J.; Meng, F. N.; Zhuang, X. Y.; Tong, D. Y. Cao, C. Atomic surface of silicon wafers induced by grafted silica nanoparticles and sodium carbonate. *Appl. Surf. Sci.* **2024**, 664, 160234-160242.

[16] Liu, D. D.; Zhang, Z. Y.; Zhou, H. X.; Deng, X. Q.; Shi, C. J.; Meng, F. N.; Yu, Z. B.; Feng, J. Y. Angstrom surface on copper induced by novel green chemical mechanical polishing using ceria and silica composite abrasives. *Appl. Surf. Sci.* **2023**, 640, 158382-158389.

[17] Zhang, Z. Y.; Liu, J.; Hu, W.; Zhang, L. Z.; Xie, W. X.; Liao, L. X. Chemical mechanical polishing for sapphire wafers using a developed slurry. *J. Manuf. Process.* **2021**, 62, 762-771.

[18] Luo, Z.; Zhang, Z. Y.; Zhou, H. X.; Yang, M.; Wang, Y. M.; Li, S. L.; Shao, J. T.; Zhang, X. B.; Liu, Z. H. A novel approach of micro-nano bubbles enhanced immersed chemical mechanical polishing on orthopedic implants with curved surface using a developed polisher. *J. Mater. Sci. Technol.* **2026**, 272, 196-207.

[19] Zhao, F.; Zhang, Z. Y.; Zhou, H. X.; Chen, L. L.; Hai, K.; Wu, L. W.; Yu, J. H.; Zhang, Z. F.; Fan, C. Unprecedented developed composite polishing system to achieve atomic surface integrating rough and fine polishing using a novel hyper-conjugated pad through controlling the temperature of a proposed green slurry. *Adv. Compos. Hybrid. Mater.* **2025**, 8, 234-251.

[20] Wang, D.; Liu, L.; Zhang, Z. Y.; Peng, Q. B.; Shi, C. J.; Liu, X. Q.; Liu, X. Y.; Zhou, H. X.; Wen, W. Atomic-scale planarization surface of quartz glass induced by novel green chemical mechanical polishing using three ingredients. *Mater. Today Sustain.* **2024**, 25, 100669-100678.

[21] Li, J. X.; Zhang, Z. Y.; Zhou, H. X.; Zhao, F.; Liu, X. Q.; Wen, W. Atomic level surface roughness of epoxy resin induced by novel chemical mechanical polishing with high material removal rate and its mechanisms elucidated using molecular dynamics simulations and density functional theory. *Nanoscale.* **2025**, 17, 16630-16645.

[22] Li, Y. R.; Zhang, Z. Y.; Zhao, F.; Yang, B.; Xuan, F. Z.; Xiang, Y. X.; Zhang, B. W.; Deng, X. Q.; Liu, Z. H. Novel full-frequency material removal models verified by polishing experiments using three kinds of polishing pads performed on a developed five-axis polisher. *Tribol. Int.* **2026**, 220, 111930-111941.

[23] Yu, Z. B.; Zhang, Z. Y.; Zeng, Z. N.; Fan, C.; Gu, Y.; Shi, C. J.; Zhou, H. X.; Meng, F. N.; Feng, J. Y. Atomic surface of diamond induced by novel green photocatalytic chemical mechanical polishing with high material removal rate. *Int. J. Extrem. Manuf.* **2025**, 7, 025102-025118.

[24] Luo, Z. Y.; Lu, J. B.; Zeng, J.; Wang, X. H.; Yan, Q. S. Experimental study on single crystal diamond CMP based on Fenton reaction and analysis of oxidation mechanism. *Mater. Sci. Semicond. Proc.* **2024**, 182, 108739-108752.

[25] Meyerstein, D. Re-examining Fenton and Fenton-like reactions. *Nat. Rev. Chem.* **2021**, 5, 595-597.

[26] Yan, Q. Y.; Zhang, J. L.; Xing, M. Y. Cocatalytic Fenton reaction for pollutant control. *Cell Rep. Phy. Sci.* **2020**, 1, 100149-100173.

[27] Kubota, A.; Yoshimura, M.; Fukuyama, S.; Iwamoto, C.; Touge, M. Planarization of C-face 4H-SiC substrate using Fe particles and hydrogen peroxide solution. *Precis. Eng.* **2012**, 36, 137-140.

[28] Lu, J. B.; Chen, R.; Liang, H. Z.; Yan, Q. S. The influence of concentration of hydroxyl radical on the chemical mechanical polishing of SiC wafer based on the Fenton reaction. *Precis. Eng.* **2018**, 52, 221-226.

[29] Xu, L. J.; Wang, J. L. Fenton-like degradation of 2,4-dichlorophenol using Fe_3O_4 magnetic nanoparticles. *Appl. Catal. B Environ.* **2012**, 123, 117-126.

[30] Wang, J. L.; Tang, J. T. Fe-based Fenton-like catalysts for water treatment: preparation, characterization and modification. *Chemosphere.* **2021**, 276, 130177-130213.

[31] Yuan, Z. W.; He, Y.; Sun, X. W.; Wen, Q. UV-TiO_2 photocatalysis-assisted chemical mechanical polishing 4H-SiC wafer. *Mater. Manuf. Process.* **2018**, 33, 1214-1222.

[32] Deng, H.; Yamamura, K. Atomic-scale flattening mechanism of 4H-SiC(0001) in plasma assisted polishing. *Cirp Ann-Manuf. Techn.* **2013**, 62, 575-578.

[33] Zhou, Y.; Pan, G. S.; Shi, X. L.; Gong, H.; Luo, G. H.; Gu, Z. H. Chemical mechanical planarization (CMP) of on-axis Si-face SiC wafer using catalyst nanoparticles in slurry. *Surf. Coat. Tech.* **2014**, 251, 48-55.

[34] Chen, S. D.; Lei, H. Polishing performance and mechanism of a novel Fe-based slurry for chemical mechanical polishing. *Tribol. Int.* **2024**, 194, 109549-109560.

[35] Ding, J. F.; Xu, C. J.; Fan, G. L.; Naren, T.; Wang, Y.; Liu, Y.; Gu, X. J.; Wu, L. M.; Zeng, S. H. Engineering CeO_2 configurations to regulate the CuO_x dispersion and switch pathways of preferential CO oxidation. *Appl. Catal. B Environ.* **2023**, 331, 122686-122699.

[36] Xing, Y.; Wu, J. X.; Zhang, C. S.; Zhang, L.; Han, J.; Liu, D. S.; Wang, H. H.; Hou, X. N.; Gao, Z. X. Mn-induced Cu/Ce catalysts with improved performance for CO preferential oxidation in H_2/CO_2-rich streams. *Int. J. Hydrogen Energy.* **2023**, 48, 20667-20679.

[37] Liu, X.; Liu, T.; Ouyang, T.; Deng, J. G.; Liu, Z. Q. Ce^{3+}/Ce^{4+} ion redox shuttle stabilized $Cu^{\delta+}$ for efficient CO_2 electroreduction to C_2H_4. *Angew. Chem. Int. Ed.* **2025**, 64, e202419796.

[38] Zhang, N. Q.; Yi, Y. Q.; Lian, J. T.; Fang, Z. Q. Effects of Ce doping on the Fenton-like reactivity of Cu-based catalyst to the fluconazole. *Chem. Eng. J.* **2020**, 395, 124897-124906.

[39] Feng, X. T.; Liu, J. Y.; Kong, Y.; Zhang, Z. X.; Zhang, Z. D.; Li, S. Z.; Tong, L, M.; Gao, X.; Zhang, J. Cu/Cu_xO/Graphdiyne tandem catalyst for efficient electrocatalytic nitrate reduction to ammonia. *Adv. Mater.* **2024**, 36, 2405660-2405667.

[40] Yu, J. C.; Xi, X. C.; Su, J. H.; Li, L.; Jing, P.; Xu, X.; Liu, B. C.; Zhang, J. A Cu-Co_3O_4 tandem catalyst for efficient electrocatalytic nitrate reduction at low concentration. *ACS Mater. Lett.* **2024**, 6, 2591-2598.

[41] Huang, B. K.; Wu, Z. L.; Zhou, H. Y.; Wang, X. H.; Liu, Y.; Zhang, H.; Xiong, Z. K.; Lai, B. The structure-performance relationships in active center

size-dependent Fenton-like catalysis: From nanoparticles to single atoms. *App. Catal. B: Environ.* **2024**, 355, 124157-124175.

[42] Zhou, J.; Sun, Y. J.; Sun, W. Q.; Hong, F. Treatment of phenol-containing coal chemical biochemical tailwater by catalytic ozonation using Mn-Ce/γ-Al_2O_3. *Catalysts.* **2022**, 12, 1019-1034.

[43] Chen, Y.; Yang, Z.; Liu, Y. B.; Liu, Y. Fenton-like degradation of sulfamerazine at nearly neutral pH using Fe-Cu-CNTs and Al_0-CNTs for in-situ generation of H_2O_2/OH/O_2^-. *Chem. Eng. J.* **2020**, 396, 125329-125339.

[44] Liu, Y.; Huang, S. X.; Sun, H. J.; Liu, Y.; Liang, L. J.; Nan, Q. W.; Wang, T.; Chen, Z. Z.; Tang, J. T.; Hu, C. B.; Zhao, J. R. Amorphous Cu-Mn hopcalite as novel Fenton-like catalyst for H_2O_2-activated degradation of tetracycline at circumneutral pH. *J. Sci. Adv. Mater. Dev.* **2023**, 8, 100603-100613.

[45] Li, T.; Wang, X. M.; Chen, Y. M.; Liang, J. R.; Zhou, L. K. Producing ·OH, SO_4^- and $\cdot O_2^-$ in heterogeneous Fenton reaction induced by Fe_3O_4-modified schwertmannite. *Chem. Eng. J.* **2020**, 393, 124735-124744.

[46] Xu, J.; Gu, K. Y.; Wang, P. F.; Cheng, P. F.; Che, H. N.; Tang, C. M. Piezo-catalytic in-site H_2O_2 generation and activation across wide pH range to drive hydroxyl radical-mediated pollutant degradation. *Nat. Commun.* **2025**, 16, 7908-7918.

[47] Hu, D.; Lu, J. B.; Yan, Q. S.; Li, H. L.; Cao, J. Y. Study of catalytic properties and grinding performance of single-crystal SiC heterogeneous Fenton reaction grinding discs. *Int. J. Adv. Manuf. Technol.* **2024**, 133, 2551-2563.

[48] Yin, X. C.; Li, S. J.; Ma, G. L.; Jia, Z.; Liu, X. Investigation of oxidation mechanism of SiC single crystal for plasma electrochemical oxidation. *RSC Adv.* **2021**, 11, 27338-27345.

[49] Luo, Q. F.; Lu, J.; Xu, X. P. A comparative study on the material removal mechanisms of 6H-SiC polished by semi-fixed and fixed diamond abrasive tools. *Wear.* **2016**, 350-351, 99-106.

[50] Asghar, K.; Qasim, M.; Nelabhotla, D. M.; Das, D. Effect of surfactant and electrolyte on surface modification of c-plane GaN substrate using chemical mechanical planarization (CMP) process. *Colloids Surf. A Physicochem. Eng. Aspects.* **2016**, 497, 133-145.

[51] Murata, J.; Hayama, K.; Takizawa, M. Environment-friendly electrochemical mechanical polishing using solid polymer electrolyte/CeO_2 composite pad for highly efficient finishing of 4H-SiC (0001) surface. *Appl. Surf. Sci.* **2023**, 625, 157190-157200.

[52] Zhang, Q. X.; Li, K. S.; Zhang, X.; Gao, R.; Cheung, C. F.; Wang, C. J. Effects of picosecond laser ablation and surface modification on the surface/interface characteristics and removal performance of 4H-SiC. *J. Mater. Sci. Technol.* **2025**, 234, 199-216.

[53] Xu, Z. W.; He, Z. D.; Song, Y.; Fu, X.; Rommel, M.; Luo, X. C.; Hartmaier, A.; Zhang, J. J.; Fang, F. Z. Topic review: application of Raman spectroscopy characterization in micro/nano-machining. *Micromachines.* **2018**, 9, 361-383.

[54] Wang, X. H.; Chen, J. P.; Bu, Z. Z.; Wang, H. Q.; Wang, W. J.; Li, W. M.; Sun, T. Accelerated C-face polishing of silicon carbide by alkaline polishing slurries with Fe_3O_4 catalysts. *J. Environ. Chem. Eng.* **2021**, 9, 106863-106872.

[55] Chen, G. M.; Ni, Z. F.; Bai, Y. W.; Li, Q. Z.; Zhao, Y. W. The role of interactions between abrasive particles and the substrate surface in chemical-mechanical planarization of Si-face 6H-SiC. *RSC Adv.* **2017**, 7, 16938-16952.

[56] Wang, W. T.; Zhang, B. G.; Shi, Y. H.; Zhou, D. K.; Wang, R. Improvement in dispersion stability of alumina suspensions and corresponding chemical mechanical polishing performance. *Appl. Surf. Sci.* **2022**, 597, 153703-153714.

[57] Bai, J.; Zhang, G. H.; Hong, G. Y.; Yu, A. B.; Li, J. Structural evolution and rheology of continuous shear-induced dense granular flow in unsteady state. *Phys. Fluids.* **2024**, 36, 053307.

[58] Yuan, J. Q.; Ding, Z.; Gong, X.; Yu, A. M.; Wen, S. M.; Bai, S. J. Degradation of residual xanthate in flotation tailing wastewater by activated H_2O_2 with natural ilmenite: A heterogeneous Fenton-like reaction catalyzed at natural PH. *Sep. Purif. Technol.* **2024**, 332, 125819-125830.

[59] Pandey, N. K.; Li, H. B.; Chudal, L.; Bui, B.; Amador, E.; Zhang, M. B.; Yu, H. M.; Chen, M. L.; Luo, X.; Chen, W. Exploration of copper-cysteamine nanoparticles as an efficient heterogeneous Fenton-like catalyst for wastewater treatment. *Mater. Today. Phys.* **2022**, 22, 100587-100600.

[60] Zhang, P. J.; Lei, H.; Zhang, Z. F.; Zhang, J. H.; Chen, S. D.; Hu, X. G. Synthesis of Al_2O_3@MnO_2 composite abrasives and their chemical mechanical polishing performance on silicon carbide (SiC). *Ceram Int.* **2024**, 50, 19935-19944.

[61] Zhu, X. X.; Gui, Y. Z. Y.; Fu, H.; Ding, J. X.; Mo, Z. C.; Jiang, X. S.; Sun, J. F.; Ban, B. Y.; Wang, L.; Chen, J. Photocatalytic assisted chemical mechanical polishing for silicon carbide using developed ceria coated diamond core-shell abrasives. *Tribol. Int.* **2024**, 197, 109827-109838.

[62] Murata, J.; Ueno, Y.; Yodogawa, K.; Sugiura, T. Polymer/CeO_2-Fe_3O_4 multicomponent core-shell particles for high-efficiency magnetic-field-assisted polishing processes. *Int. J. Mach. Tool. Man.* **2016**, 101, 28-34.

[63] Murata, J.; Yodogawa, K.; Ban, K. Polishing-pad-free electrochemical mechanical polishing of single-crystalline SiC surfaces using polyurethane-CeO_2 core-shell particles. *Int. J. Mach. Tool. Man.* **2017**, 114, 1-7.

[64] Shen, Y.; Wang, H. X.; Guo, X. G.; Gao, S. Environment-friendly chemical mechanical polishing using $NaHCO_3$-activated H_2O_2 slurry for highly efficient finishing of 4H-SiC (0001) surface. *J. Manuf. Processes.* **2024**, 109, 213-221.

[65] Kanyal, S. S.; Jensen, D. S.; Zhu, Z. H.; Linford, M. R. Silicon (100)/SiO_2 by TOF-SIMS. *Surf. Sci. Spectra.* **2015**, 22, 1-6.

Electronic Supplementary Material

Chemical mechanical polishing on silicon carbide using developed ceria composite abrasives and their synergistic polishing mechanism

Juan Liang[1,§], Yan Zhang[1,§], Zhaokang Li[1], Peng Lv[1], Wenhao Qi[1], Hong Feng[1], Xuan Xu[1,2] ✉, Baocang Liu[1,2], Tao Bai[3], Peng Jing[1,2] ✉, and Jun Zhang[1,4] ✉

[1] *School of Chemistry and Chemical Engineering, Inner Mongolia University, 49 Xilinguole South Road, Hohhot 010020, China*
[2] *Inner Mongolia Key Laboratory of Rare Earth Catalysis, Inner Mongolia University, 49 Xilinguole South Road, Hohhot 010020, China*
[3] *Inner Mongolia Guangheyuan Nano High Tech Co., Ltd., 22 Sarula North Road, Ordos 017010, China*
[4] *School of Chemistry and Environmental Science, Inner Mongolia Normal University, 81 Zhaowuda Road, Hohhot 010022, China*
[§] *Juan Liang and Yan Zhang contributed equally to this work.*

✉ Address correspondence to Xuan Xu, xu.xuan@imu.edu.cn; Peng Jing, pjing@imu.edu.cn; Jun Zhang, cejzhang@imu.edu.cn

Supporting information to https://doi.org/10.26599/NR.2026.94909100

1. Materials and Methods

1.1. Materials

Cerium nitrate ($Ce(NO_3)_3·6H_2O$, 99.9%), copper nitrate ($Cu(NO_3)_2·3H_2O$, 99.9%), aqueous ammonia ($NH_3·H_2O$, 25 wt.%), and rhodamine B ($C_{28}H_{31}ClN_2O_3$, RhB, 99.7%) were purchased from Beijing Innochem Technology Co., Ltd. Hydrogen peroxide (H_2O_2, 30 wt.%) was purchased from Sinopharm Chemical Reagents Co., Ltd. Al_2O_3 abrasives (99.9%) was purchased from China Metallurgical New Materials Technology Co., Ltd. All chemical reagents were used directly without further purification.

1.2. Characterizations

X-ray diffraction (XRD) analysis was performed using a diffractometer (Panalytical, Netherlands) with Cu Kα radiation (λ = 0.15460 nm). Scanning electron microscopy (SEM) was performed using a scanning electron microscope (TESCAN MIRA LMS, Czech). Transmission electron microscopy (TEM) was performed using a transmission electron microscope (FEI Talos F200X G2, USA). X-ray photoelectron spectroscopy (XPS) was performed on a spectrometer (Thermo Scientific ESCALAB Xi+, USA), all spectra were calibrated against C 1s main peak at 284.8 eV. The element content was analyzed by inductively coupled plasma-optical emission spectrometry (ICP-OES, Agilent-5110, USA). Electron paramagnetic resonance (EPR) spectra were recorded using an electron paramagnetic resonance spectrometer (Bruker EMXplus, Germany). The surface quality of SiC was measured using a white light interferometer (UP-2000, Yantai, China). Raman spectra (LabRAM HR Evolution, Japan) were performed using a 532 nm laser excitation to characterize the surface damaged layer of SiC. Elemental fragment distribution signals on the material surface were analyzed using a time-of-flight secondary ion mass spectrometer (TOF-SIMS) (TESCAN GAIA3, Czech). The absorption spectra of RhB aqueous solution before and after degradation were tested using a UV-vis spectrophotometer (Shimadzu 2600i, Japan) in the range of 200-800 nm. The Zeta potential was measured on a ZTS1240 Zeta Potential Transfer Standard particle size/potential meter (Panalytical, Netherlands). The static contact angle of the polishing slurry and SiC was tested using a video contact angle measuring instrument (JY-82C, Chengde, China). The friction wear tester (Brook UMT-5, USA) was used to test the friction performance of SiC in different polishing slurries through pin-on-disk contact.

1.3. Synthesis of composite abrasives

An appropriate amount of $Cu(NO_3)_2·3H_2O$, $Ce(NO_3)_3·6H_2O$ and 15.00 g of Al_2O_3 were uniformly dispersed in deionized water (100.00 g). After ultrasonic treatment for 30 min, $NH_3·H_2O$ was gradually added to the mixture and the solution was stirred at 90 °C for 8 h. The precipitate was then separated by centrifugation, washed five times with deionized water, dried at 90°C, and

calcined at 500 °C in air for 2 h to yield Cu_xO-CeO_2/Al_2O_3 composite abrasives. Several control samples (CeO_2/Al_2O_3 and Cu_xO/Al_2O_3) were synthesized using a similar procedure, with variations in the molar ratios of the raw materials (**Table S1 in the ESM**). Cu_xO-CeO_2/Al_2O_3 was used to represent Cu_xO-CeO_2/Al_2O_3 composite abrasives with Cu:Ce molar ratio of 2:1 throughout the text unless otherwise noted.

1.4. Catalytic performance of composite abrasives for RhB degradation

To measure the concentration of radicals, a color indicator (RhB) was employed as a probe. 20 mg of the sample was added to 50 mL of a RhB aqueous solution (20 mg/L) and stirred for 30 min to reach adsorption-desorption equilibrium. Subsequently, 40 mM H_2O_2 (0.2 mL) was introduced to the above solution, and the pH was adjusted to desired value using 1 mol/L NaOH or 1 mol/L HNO_3. 2.0 mL of the solution was extracted from the reactor every 10 min and filtered through an organic nylon membrane (0.22 μm), the absorbance of the RhB solution was measured at 554 nm using a UV-vis spectrophotometer and the corresponding concentration was then calculated according to standard curves (**Fig. S8 in the ESM**). The degradation efficiency of the RhB solution was determined using **Eq. (S1) in the ESM**, where C_0 is the initial concentration of RhB (mg/L), and C_t is the concentration of RhB after reaction (mg/L).

$$\text{Degradation efficiency (\%)} = [(C_0-C_t) / C_0] \times 100\% \quad (S1)$$

Eq. (S2) in the ESM is a pseudo-first-order reaction kinetic model, where k is kinetic constant (min^{-1}) and t is the reaction time (min).

$$\ln(C_t) = -kt + \ln(C_0) \quad (S2)$$

1.5. Polishing tests

The polishing slurry was prepared using 5 wt.% of abrasives, 8 wt.% of H_2O_2, and 87 wt.% of deionized water. Prior to the polishing test, the pH of slurry was adjusted to desired value using 1 mol/L NaOH or 1 mol/L HNO_3, and then subjected to ultrasonic treatment for 30 min. The SiC was a 2-inch (50.8 mm) conductive 4H-SiC produced by Jingdian New Materials Co., Ltd. Prior to the experiment, the gravity sample holder was placed on a heating stage at 80 °C for 3 min. The SiC, which had been cleaned with anhydrous ethanol, was adhered to the center of the sample holder using paraffin wax. After applying pressure with a weight for 1 min, the sample holder was cooled to room temperature.

Polishing tests were performed on SiC by UNIPOL-1200S CMP equipment (Shenyang Kejing Co. Ltd.) (**Fig. S10 in the ESM**). The polishing parameters were set as follows: polishing speed: 90 r/min, polishing pressure: 30 KPa, flow rate of polishing slurry: 30 mL/min, polishing time: 60 min. MRR was calculated by the following **Eq. (S3) in the ESM**, where ρ is the density of SiC (3.2 g/cm^3), s is the area of the wafer, t is polishing time, m_0 is the original mass of the wafer and m_1 is mass of the wafer after polishing. After polishing, Sa measurement was conducted using a white light interferometer, with a measurement range of 50 × 50 μm^2.

$$MRR = (m_0-m_1) / \rho st \quad (S3)$$

1.6. Radical tests

20 mg of Cu_xO-CeO_2/Al_2O_3 composite abrasives and 40 mM H_2O_2 (0.2 mL) were added to three groups of RhB aqueous solutions (20 mg/L, 50.0 mL), and the pH of the solutions was adjusted to 7. Subsequently, p-benzoquinone (1 mM, BQ, $\cdot O_2^-$ scavenger), isopropanol (1 mM, IPA, ·OH scavenger), and a blank control were added to the three solutions, respectively. The addition of radical scavengers reduces the oxidative capacity of the system, thereby identifying the primary active species during reaction.

EPR was employed to further detect the active radicals. To detect ·OH, the abrasives (5 mg/mL), 20 mM of $C_6H_{11}NO$ (DMPO), and 2 mM of H_2O_2 were added to 1 mL of H_2O. For the detection of $\cdot O_2^-$, methanol was used as the solvent, as $\cdot O_2^-$ undergoes a disproportionation reaction in water to produce H_2O and O_2, while other experimental conditions remained unchanged.

1.7. Friction tests

A pin-on-disk method was employed for the friction test. The friction pair consists of a fixed sample, such as a SiC wafer, and a movable friction body, such as a polishing pad or steel pin. When a specific pressure is applied, the friction body contacts the sample surface, simulating the frictional forces encountered in actual polishing process *via* reciprocating motion or rotation.

The experiment evaluates the impact of different polishing slurries on tribological behavior, as reflected in changes to the friction coefficient.

As illustrated in **Fig. S24 in the ESM**, a SiC sample with a side length of 10 mm was fixed to the bottom of the experimental container. A polyurethane polishing pad, with a diameter of 8 mm, was attached to a steel pin, forming a friction pair with the SiC, which was immersed in the polishing slurry. The friction pair was driven by an electric motor to perform linear reciprocating motion along the X-axis. To closely replicate the polishing condition, the following parameters were employed: a pressure of 30 KPa, a friction speed of 4 mm/s, a friction path of 8 mm, and a friction time of 10 min.

2. Figures and Tables

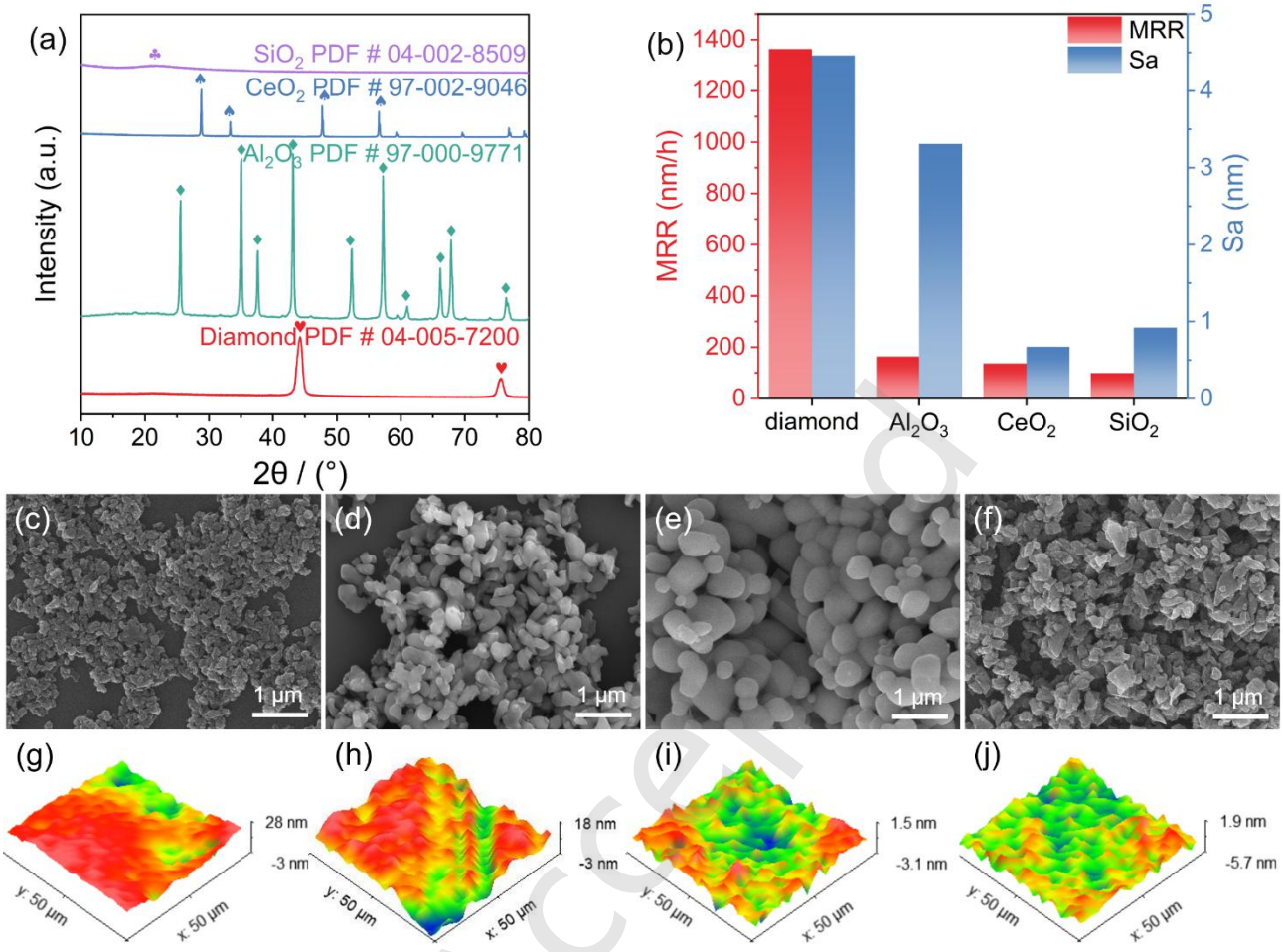

Figure S1. (a) XRD, (b) polishing performance of the four commercial abrasives. SEM images of (c) diamond, (d) Al_2O_3, (e) CeO_2, and (f) SiO_2. 3D surface images of SiC after polishing with different abrasives: (g) diamond, (h) Al_2O_3, (i) CeO_2, and (j) SiO_2.

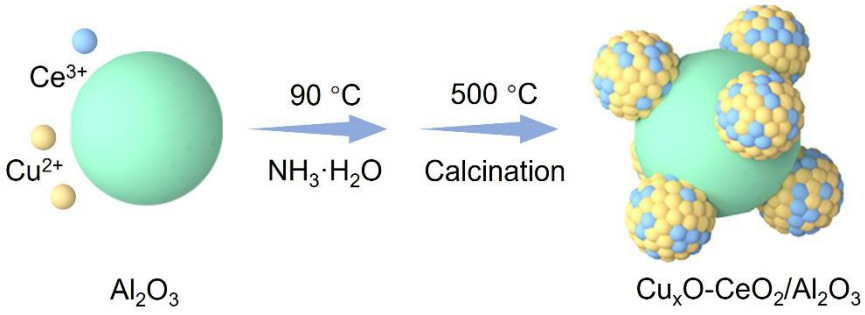

Figure S2. Synthetic route of Cu_xO-CeO_2/Al_2O_3 composite abrasives.

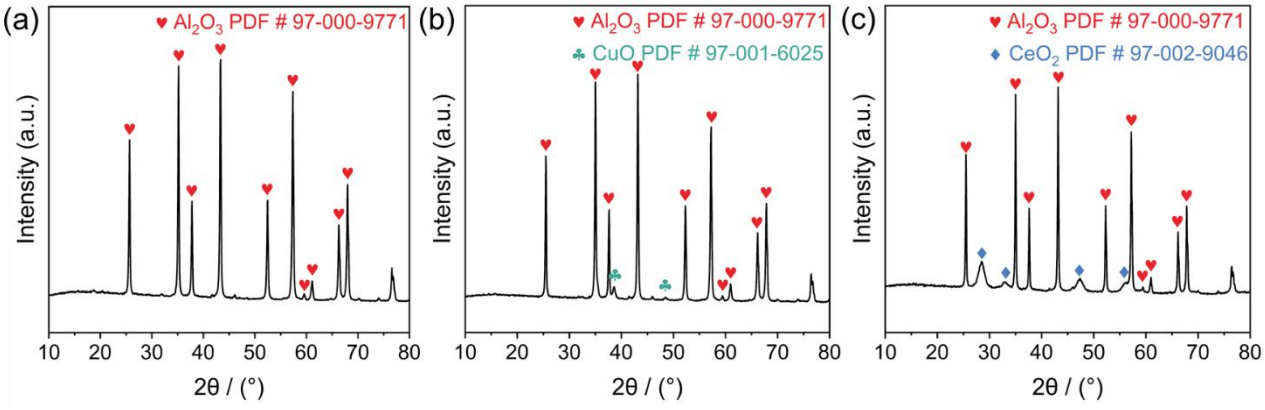

Figure S3. XRD patterns of (a) Al_2O_3, (b) Cu_xO/Al_2O_3, and (c) CeO_2/Al_2O_3 composite abrasives.

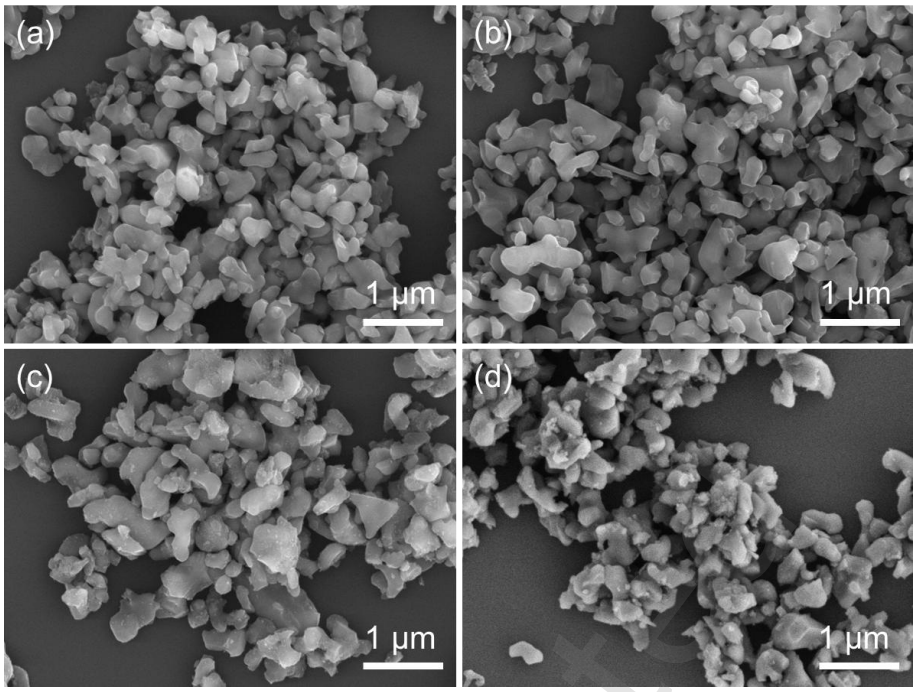

Figure S4. SEM images of (a) Al_2O_3, (b) Cu_xO/Al_2O_3, (c) CeO_2/Al_2O_3, and (d) Cu_xO-CeO_2/Al_2O_3 composite abrasives.

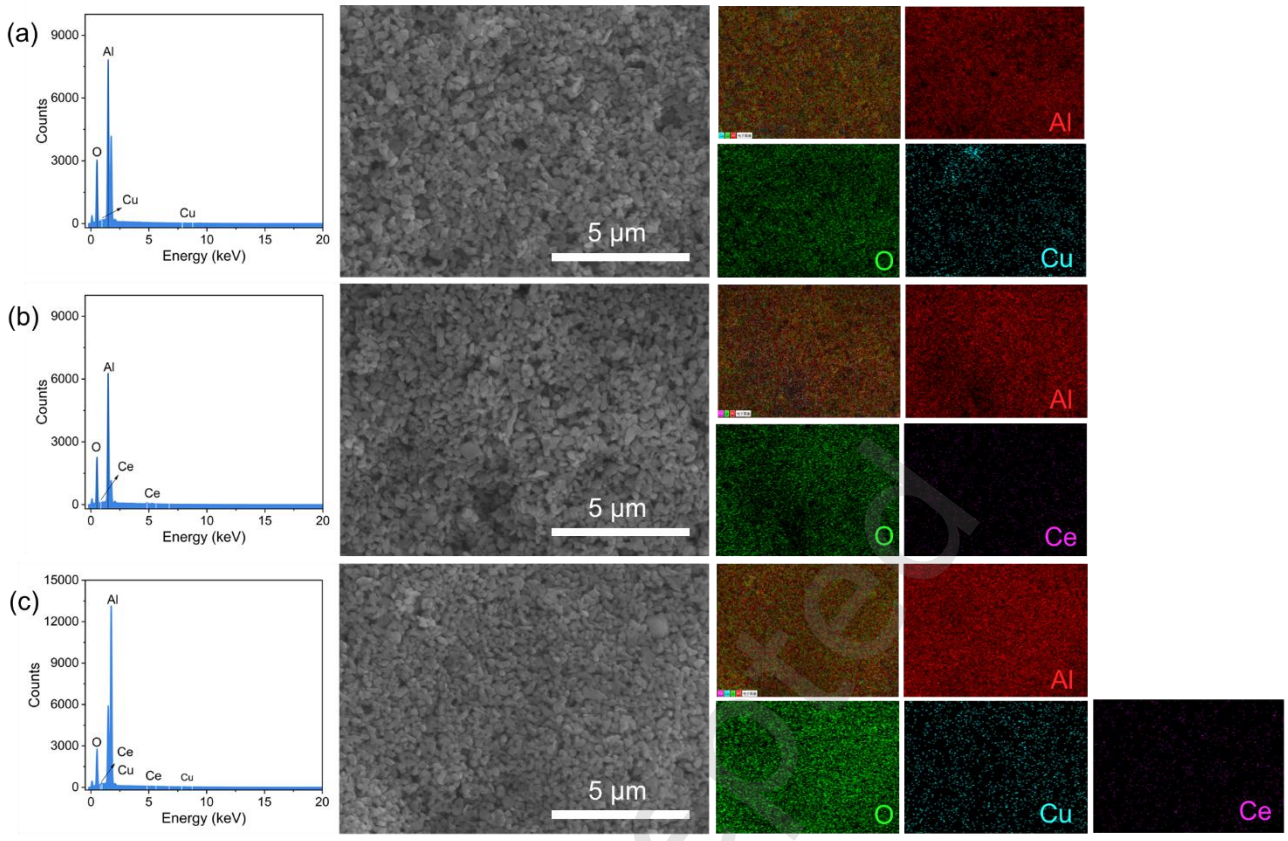

Figure S5. EDS elemental mapping images of (a) Cu_xO/Al_2O_3, (b) CeO_2/Al_2O_3, and (c) Cu_xO-CeO_2/Al_2O_3 composite abrasives.

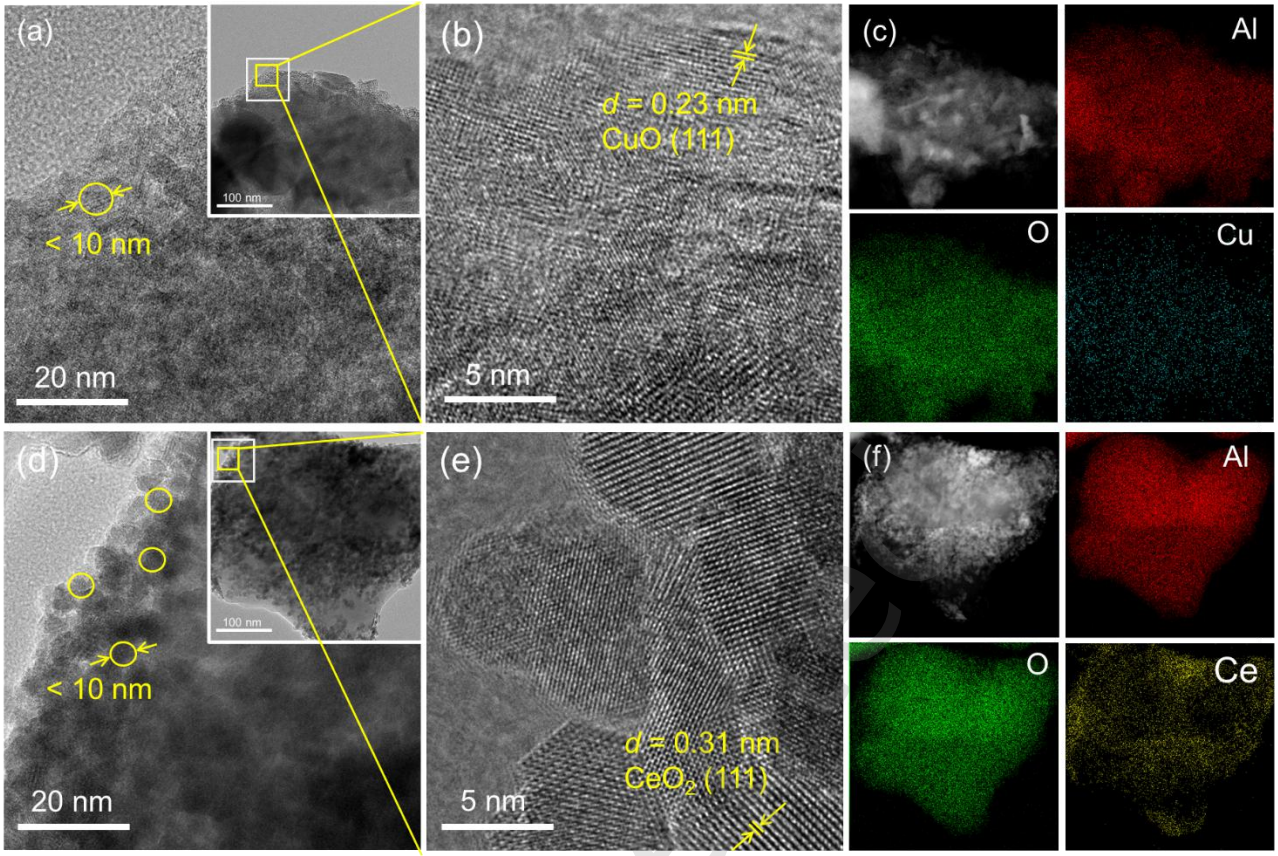

Figure S6. (a) TEM, (b) HRTEM, and (c) EDS elemental mapping images of Cu_xO/Al_2O_3 composite abrasives. (d) TEM, (e) HRTEM, and (f) EDS elemental mapping images of CeO_2/Al_2O_3 composite abrasives. The insets in (a) and (d) are the region where TEM was performed at 100 nm.

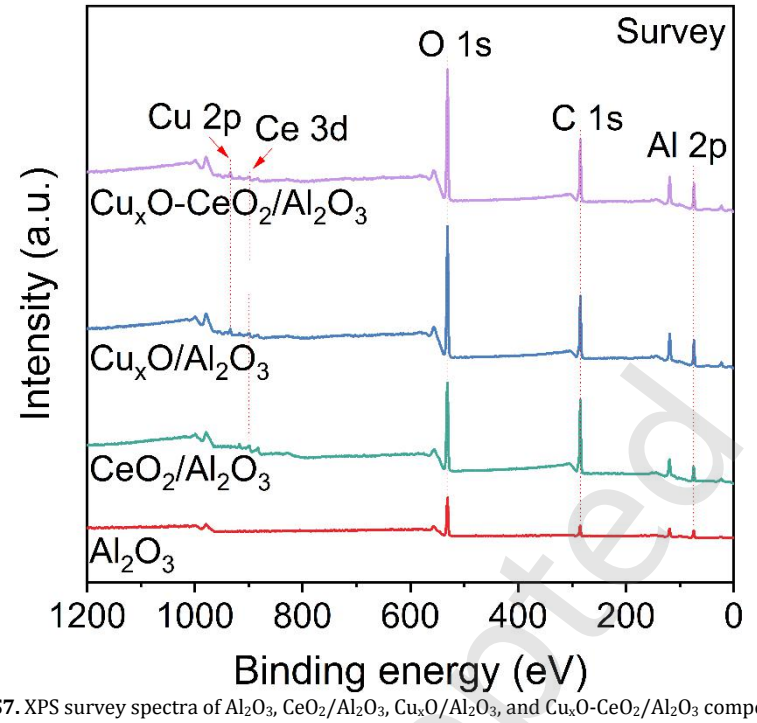

Figure S7. XPS survey spectra of Al_2O_3, CeO_2/Al_2O_3, Cu_xO/Al_2O_3, and Cu_xO-CeO_2/Al_2O_3 composite abrasives.

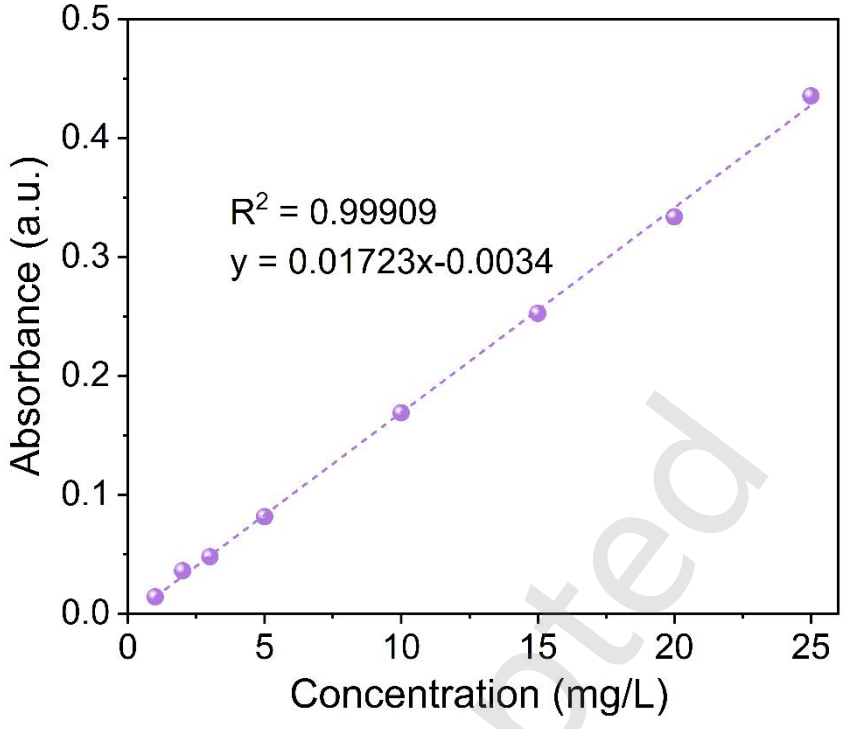

Figure S8. Linear calibration curve of the absorbance of RhB solution at 554 nm versus concentration.

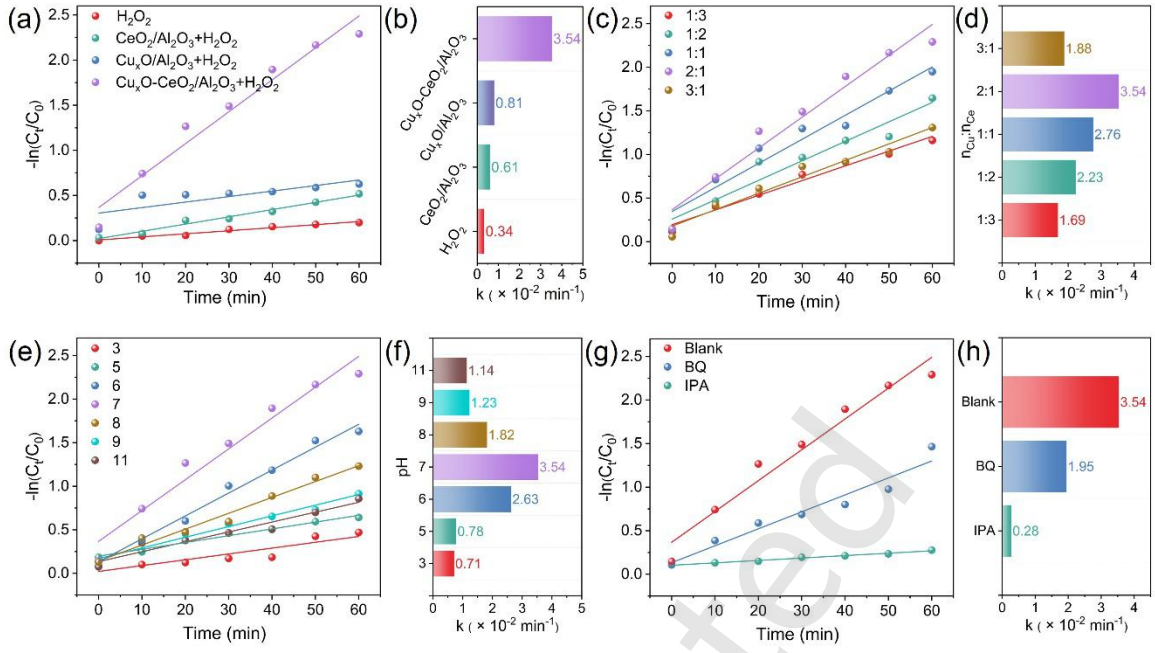

Figure S9. The pseudo first-order kinetic fitting curve and corresponding RhB degradation reaction rate constant (k) using (a, b) different abrasives, (c, d) Cu_xO-CeO_2/Al_2O_3 composite abrasives with different Cu:Ce molar ratios, (e, f) Cu_xO-CeO_2/Al_2O_3 composite abrasives at different pH values, and (g, h) Cu_xO-CeO_2/Al_2O_3 composite abrasives with different scavengers at pH of 7.

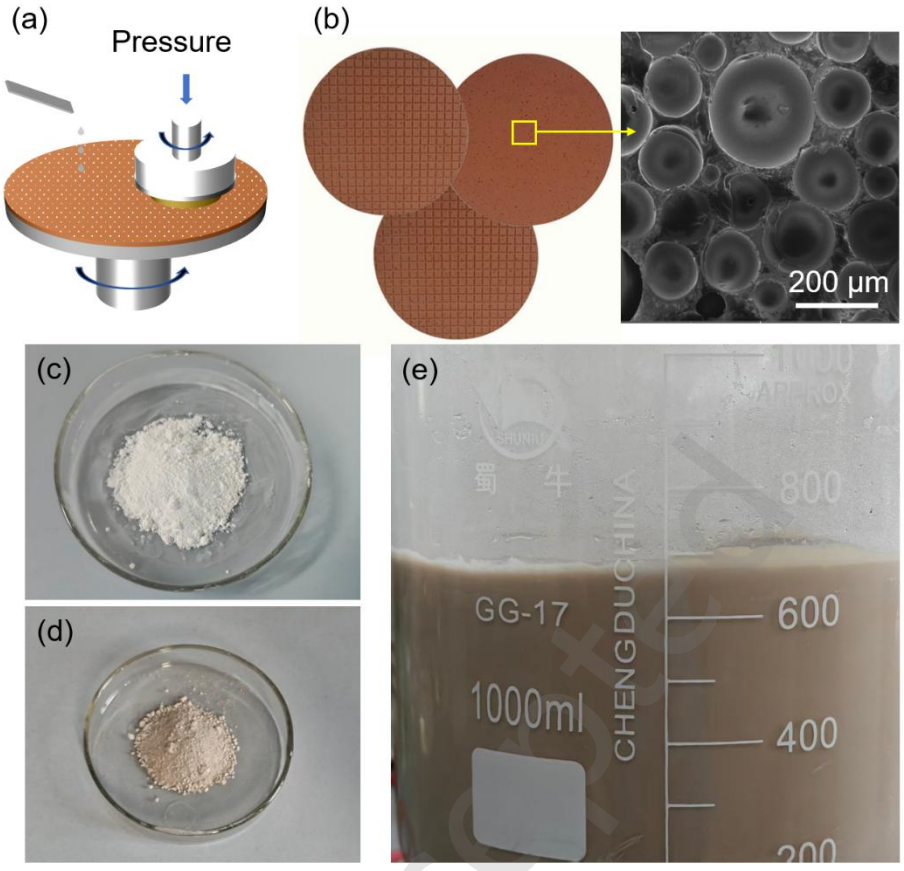

Figure S10. (a) Polishing equipment, (b) polyurethane polishing pad. Photographs of (c) Al_2O_3 abrasives, (d) Cu_xO-CeO_2/Al_2O_3 composite abrasives, and (e) Cu_xO-CeO_2/Al_2O_3 polishing slurry.

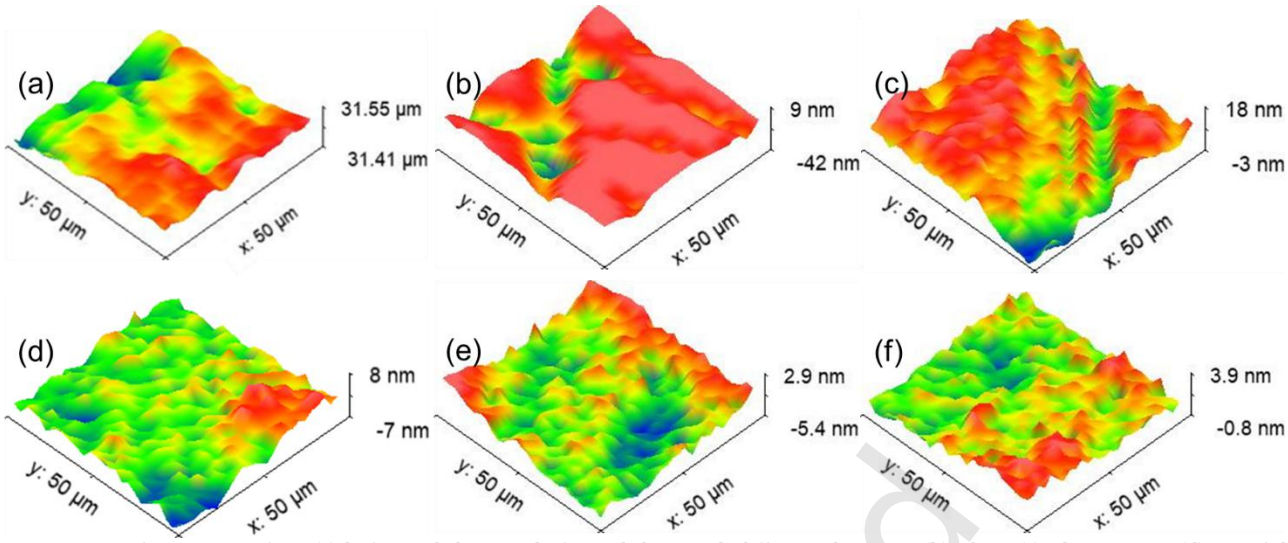

Figure S11. 3D surface images of SiC (a) before polishing, and after polishing with different abrasives: (b) Al_2O_3, (c) Al_2O_3 + H_2O_2, (d) CeO_2/Al_2O_3 + H_2O_2, (e) Cu_xO/Al_2O_3 + H_2O_2, and (f) Cu_xO-CeO_2/Al_2O_3 + H_2O_2.

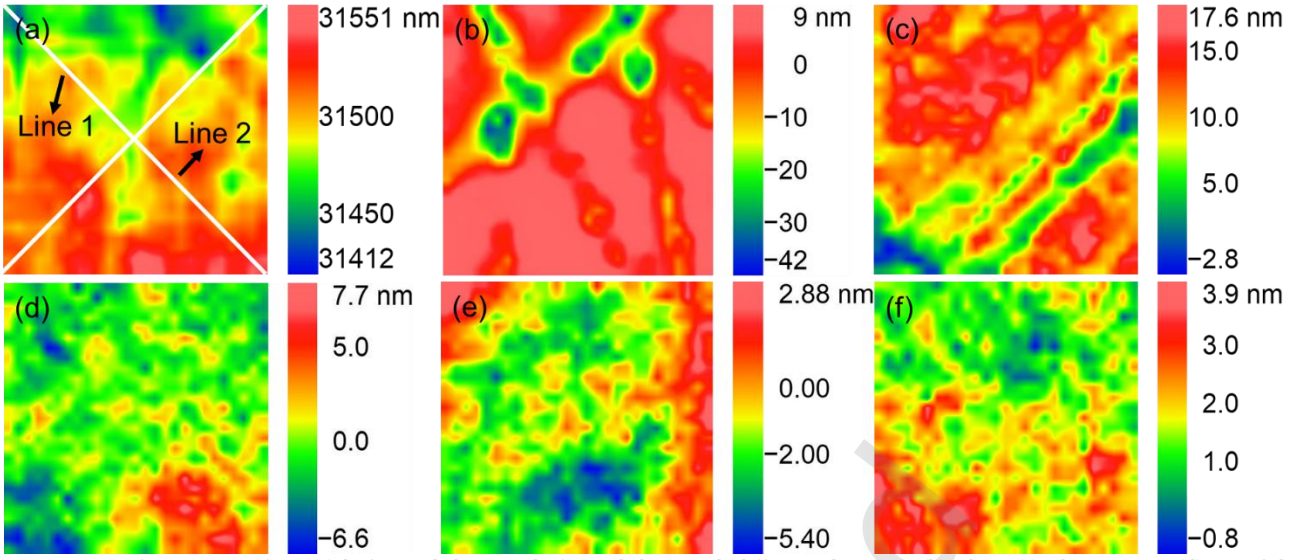

Figure S12. 2D surface images of SiC (a) before polishing, and after polishing with different abrasives: (b) Al_2O_3, (c) Al_2O_3 + H_2O_2, (d) CeO_2/Al_2O_3 + H_2O_2, (e) Cu_xO/Al_2O_3 + H_2O_2, and (f) Cu_xO-CeO_2/Al_2O_3 + H_2O_2.

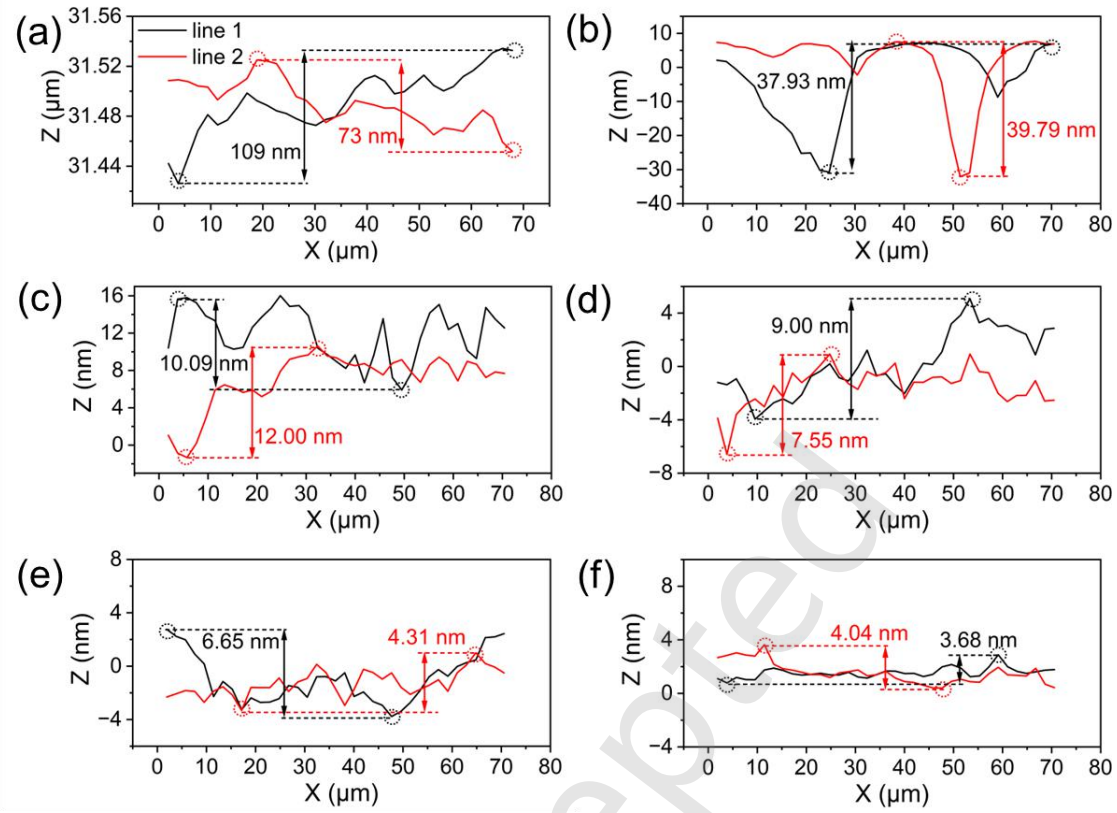

Figure S13. Height difference profiles of SiC (obtained from Fig. S12) (a) before polishing, and after polishing with different abrasives: (b) Al_2O_3, (c) $Al_2O_3 + H_2O_2$, (d) $CeO_2/Al_2O_3 + H_2O_2$, (e) $Cu_xO/Al_2O_3 + H_2O_2$, and (f) Cu_xO-$CeO_2/Al_2O_3 + H_2O_2$.

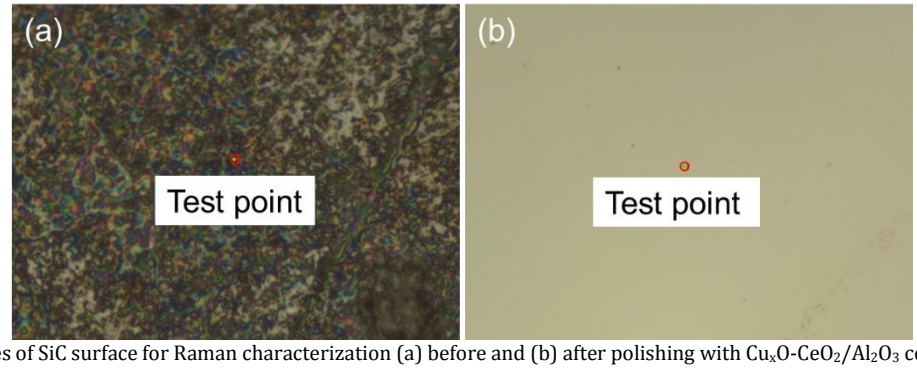

Figure S14. Images of SiC surface for Raman characterization (a) before and (b) after polishing with Cu_xO-CeO_2/Al_2O_3 composite abrasives.

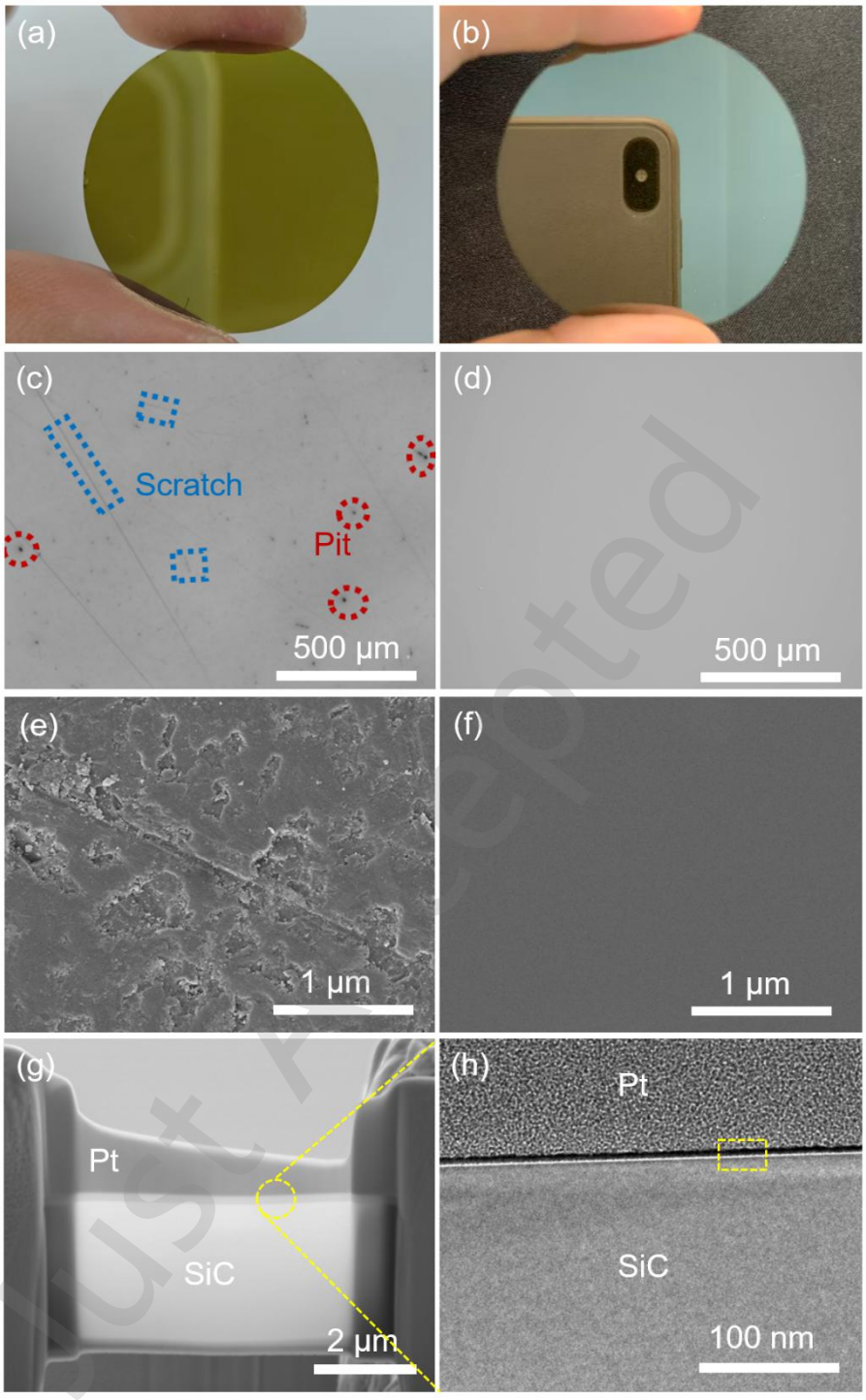

Figure S15. Photographs of SiC surface (a) before and (b) after polishing. Optical morphology images of SiC surface (c) before and (d) after polishing. SEM images of SiC surface (e) before and (f) after polishing. (g, h) Cross-sectional TEM images of SiC after polishing. Cu_xO-CeO_2/Al_2O_3 composite abrasives were used for SiC polishing.

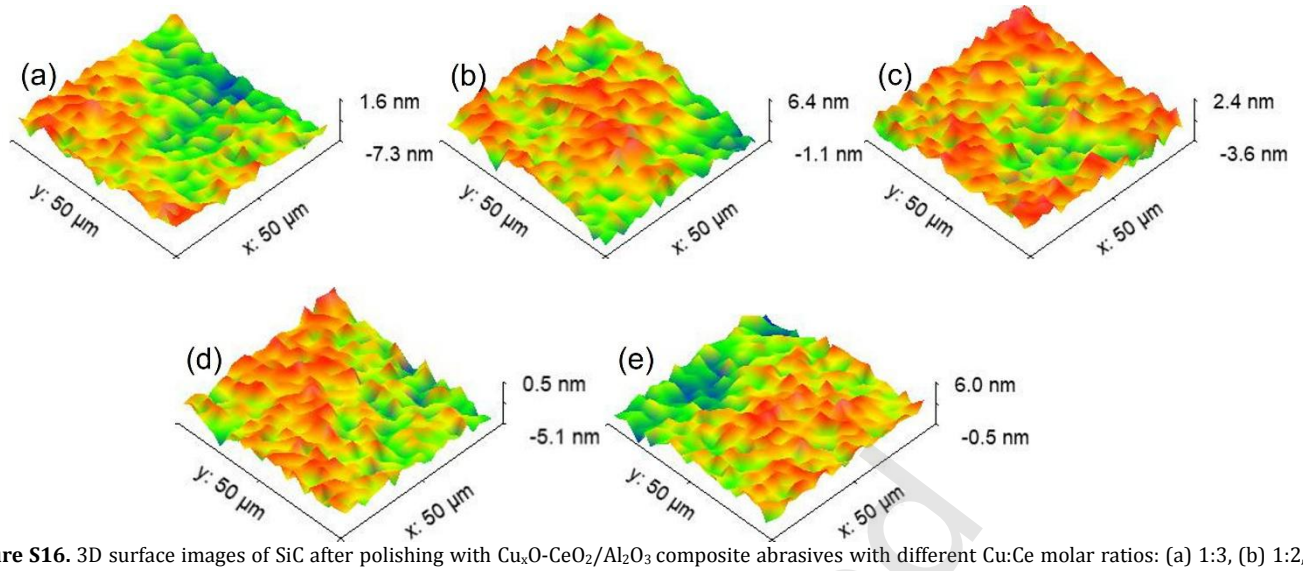

Figure S16. 3D surface images of SiC after polishing with Cu_xO-CeO_2/Al_2O_3 composite abrasives with different Cu:Ce molar ratios: (a) 1:3, (b) 1:2, (c) 1:1, (d) 2:1, and (e) 3:1.

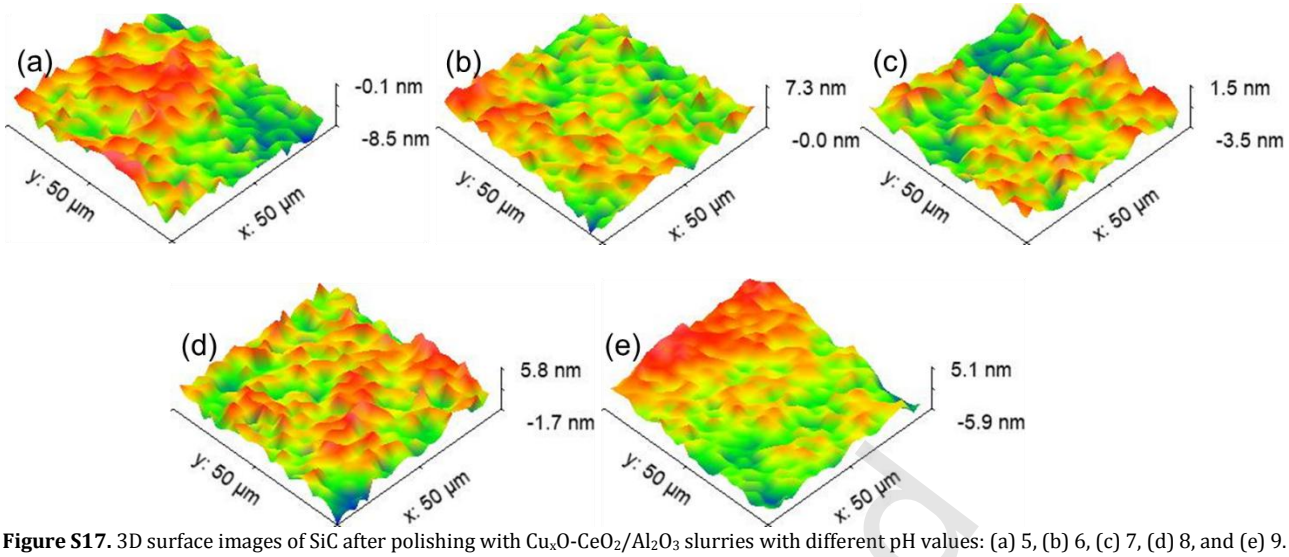

Figure S17. 3D surface images of SiC after polishing with Cu_xO-CeO_2/Al_2O_3 slurries with different pH values: (a) 5, (b) 6, (c) 7, (d) 8, and (e) 9.

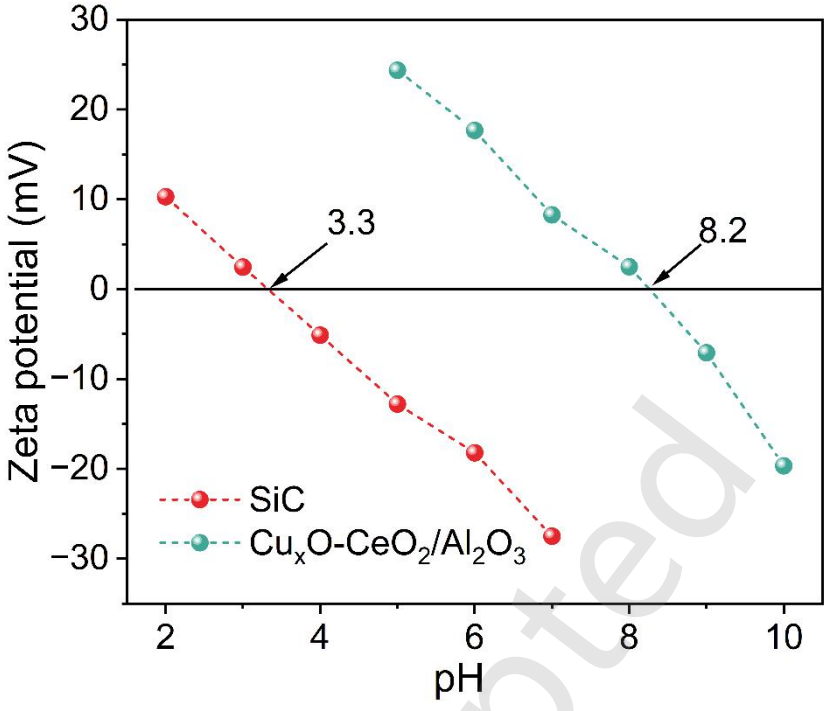

Figure S18. Zeta potentials of SiC and Cu_xO-CeO_2/Al_2O_3 polishing slurry at different pH values.

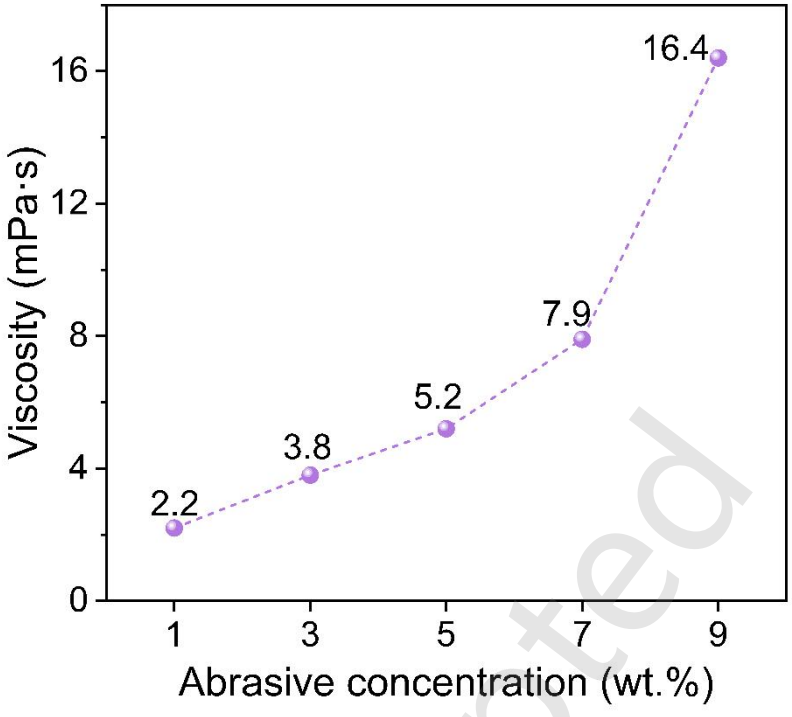

Figure S19. Viscosity of Cu_xO-CeO_2/Al_2O_3 polishing slurries with different abrasive concentrations.

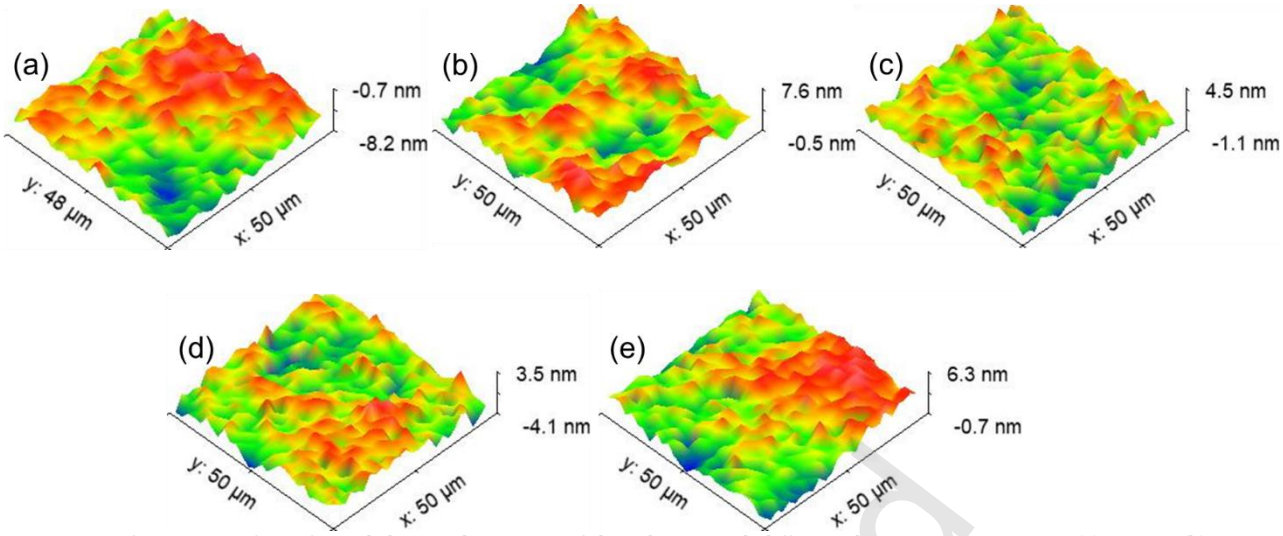

Figure S20. 3D surface images of SiC after polishing with Cu_xO-CeO_2/Al_2O_3 slurries with different abrasive concentrations: (a) 1 wt.%, (b) 3 wt.%, (c) 5 wt.%, (d) 7 wt.%, and (e) 9 wt.%.

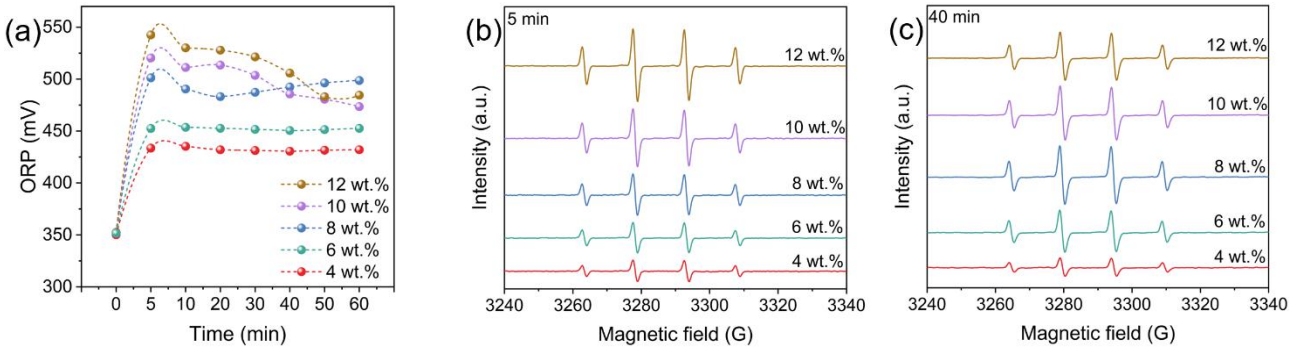

Figure S21. (a) ORP curves, and corresponding DMPO-trapped EPR spectra of Cu_xO-CeO_2/Al_2O_3 composite abrasives after (b) 5 min and (c) 40 min with different H_2O_2 concentrations.

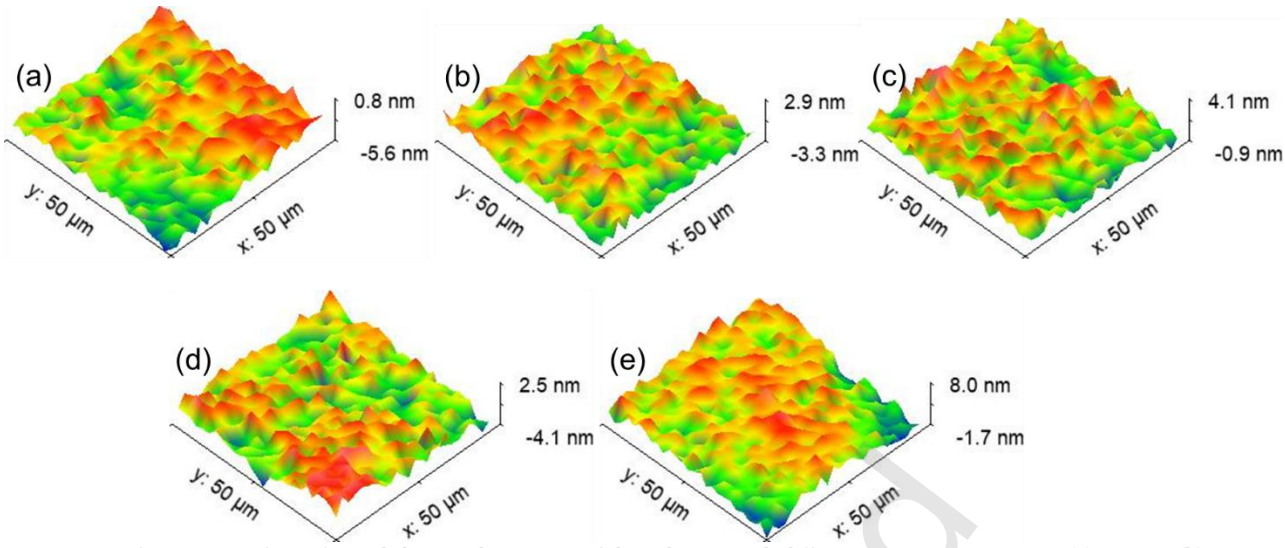

Figure S22. 3D surface images of SiC after polishing with Cu_xO-CeO_2/Al_2O_3 slurries with different H_2O_2 concentrations: (a) 4 wt.%, (b) 6 wt.%, (c) 8 wt.%, (d) 10 wt.%, and (e) 12 wt.%.

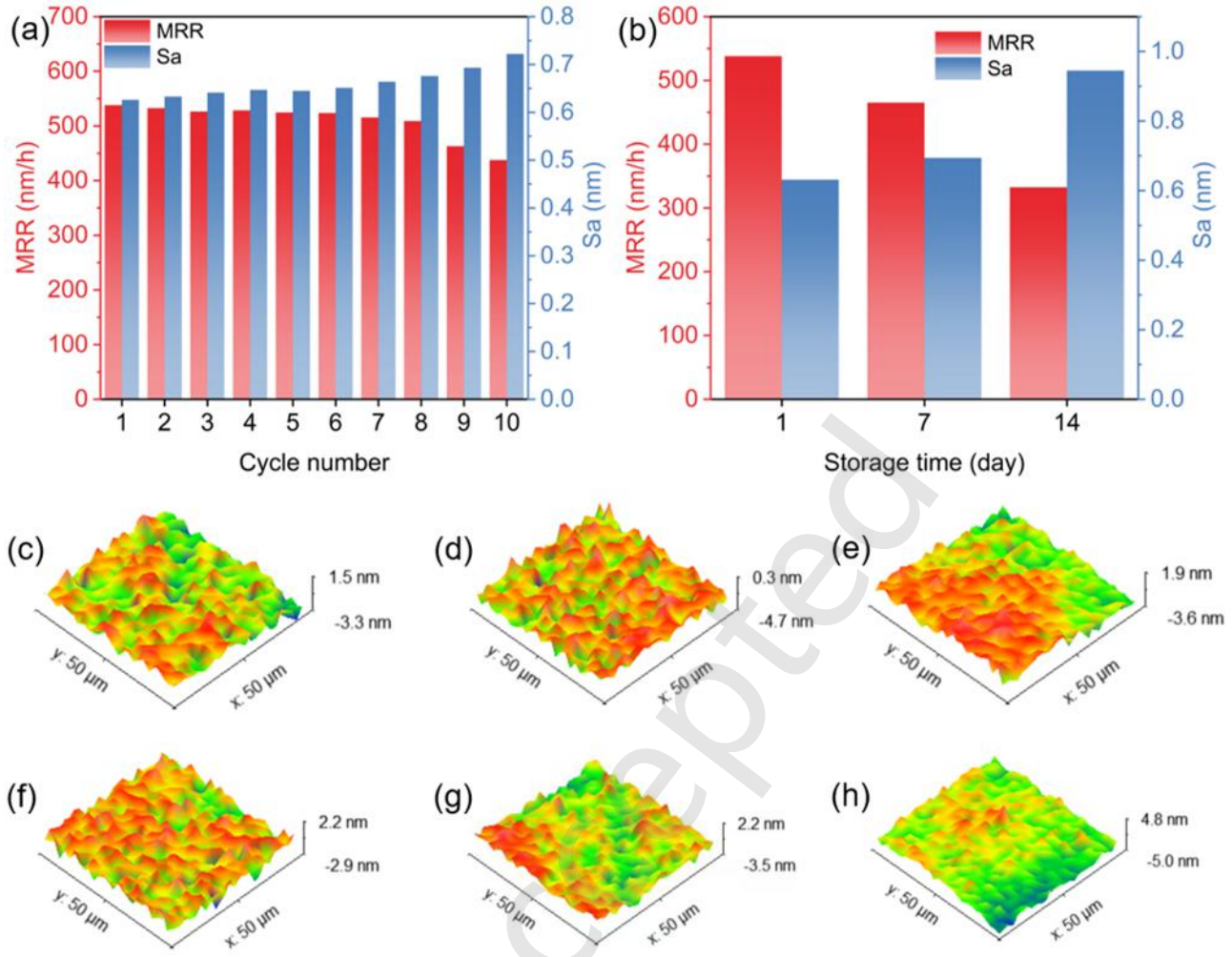

Figure S23. (a) Polishing performance of Cu_xO-CeO_2/Al_2O_3 slurry for SiC during 10 consecutive cycles. (b) Effect of storage time on the polishing performance of Cu_xO-CeO_2/Al_2O_3 slurry for SiC. 3D surface images of SiC after polishing with the reused slurry for (c) 1 cycle, (d) 5 cycles, and (e) 10 cycles. 3D surface images of SiC after polishing with the reused slurry stored for (f) 1 day, (g) 7 days, and (h) 14 days.

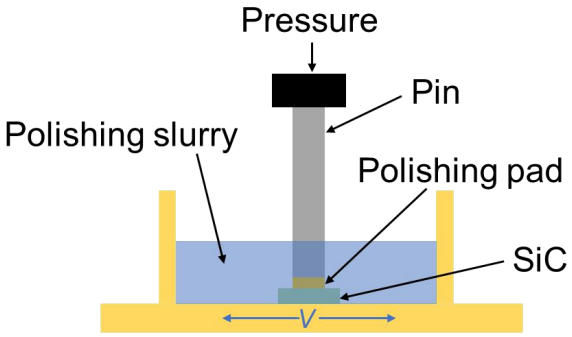

Figure S24. Pin-on-disk friction test diagram.

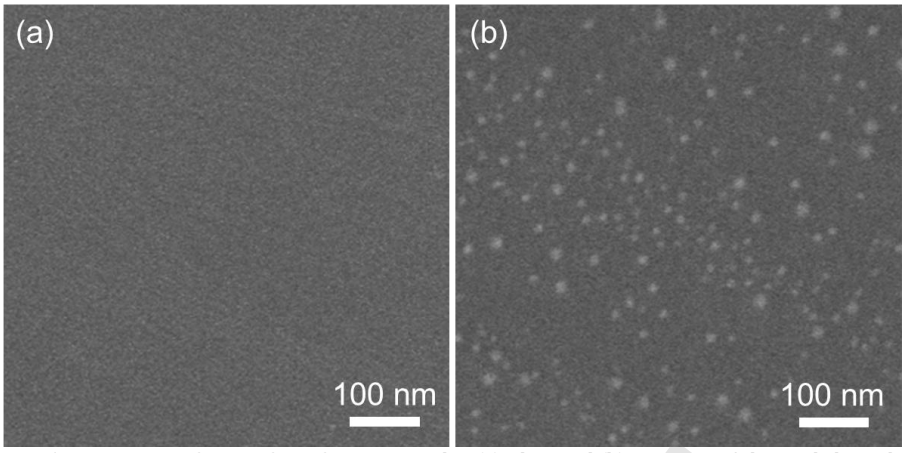

Figure S25. SEM images of SiC surface after immersed in (a) Al_2O_3 and (b) Cu_xO-CeO_2/Al_2O_3 polishing slurries.

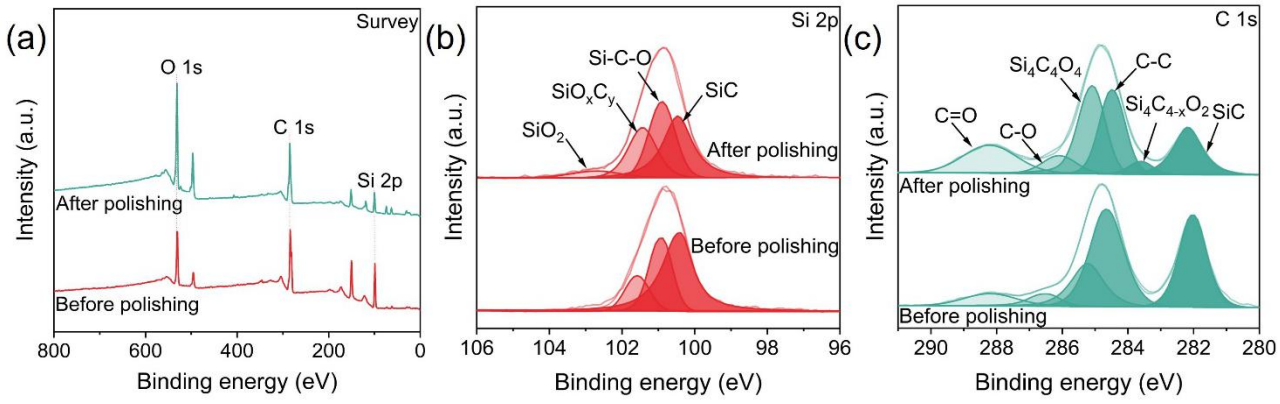

Figure S26. (a) XPS survey, (b) Si 2p, and (c) C 1s XPS spectra of SiC before and after polishing with Cu_xO-CeO_2/Al_2O_3 composite abrasives.

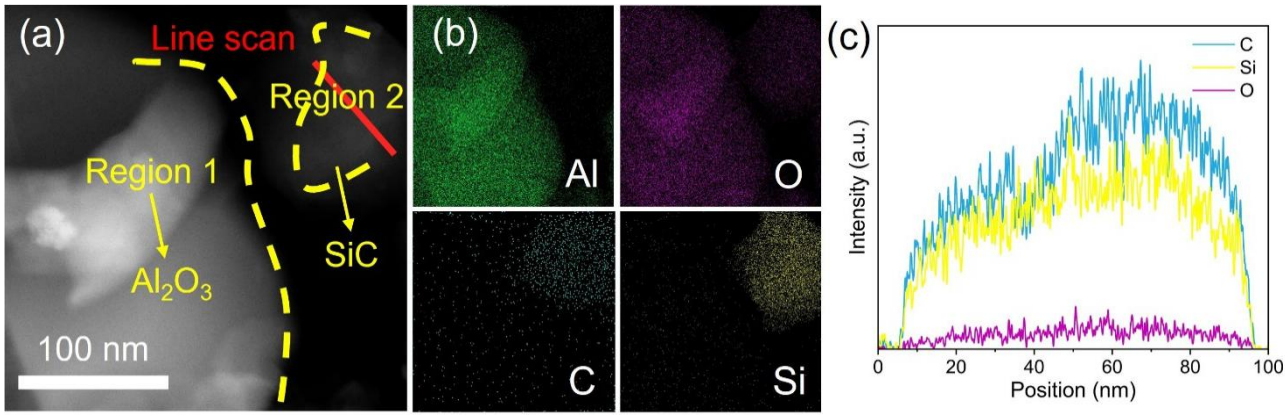

Figure S27. (a) TEM image, EDS elemental (b) mapping images, and (c) line scan profiles of SiC debris after polishing with Al_2O_3 abrasives.

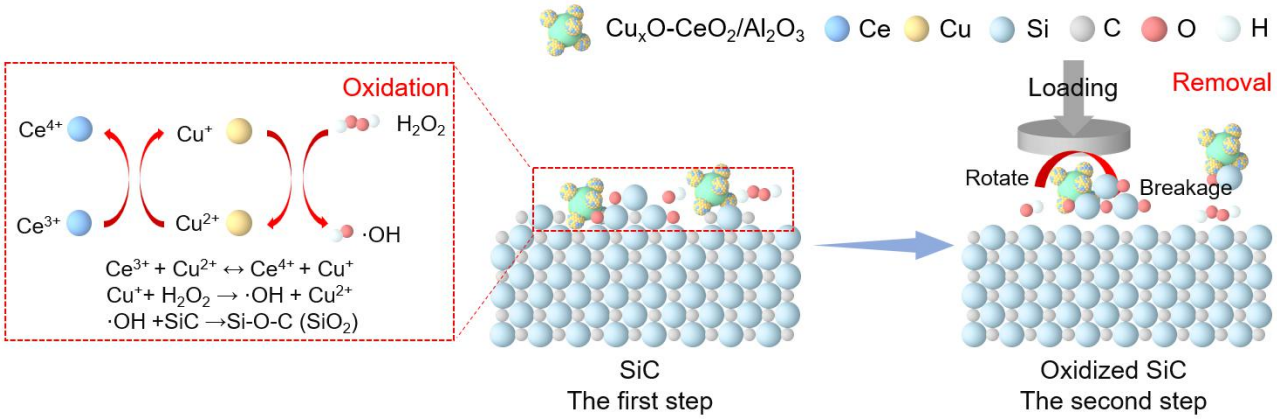

Figure S28. Atomic model of CMP mechanism for SiC with Cu_xO-CeO_2/Al_2O_3 composite abrasives.

Table S1. Synthetic conditions of various abrasives.

	$Cu(NO_3)_2 \cdot 3H_2O$ (mmol)	$Ce(NO_3)_3 \cdot 6H_2O$ (mmol)	Al_2O_3 (g)	$NH_3 \cdot H_2O$ (mmol)
Al_2O_3	0	0	15.00	0
Cu_xO/Al_2O_3	5	0	15.00	10
CeO_2/Al_2O_3	0	5	15.00	15
Cu_xO-CeO_2/Al_2O_3 (1:3)	1.25	3.75	15.00	13.75
Cu_xO-CeO_2/Al_2O_3 (1:2)	1.67	3.33	15.00	13.33
Cu_xO-CeO_2/Al_2O_3 (1:1)	2.5	2.5	15.00	12.5
Cu_xO-CeO_2/Al_2O_3 (2:1)	3.33	1.67	15.00	11.67
Cu_xO-CeO_2/Al_2O_3 (3:1)	3.75	1.25	15.00	11.25

Table S2. Theoretical (actual) contents and load efficiency of Cu and Ce.

	Cu (wt.%)			Ce (wt.%)		
	Theoretical	Actual	Ratio	Theoretical	Actual	Ratio
Cu_xO/Al_2O_3	1.96	1.78	90.82%			
CeO_2/Al_2O_3				4.08	3.82	93.63%
Cu_xO-CeO_2/Al_2O_3	1.41	1.09	77.30%	1.28	1.03	80.47%

Table S3. Comparison of polishing performance of Cu_xO-CeO_2/Al_2O_3 composite abrasives for SiC with reported abrasives (strategies).

Polishing slurry	External field	MRR (nm/h)	Sa (nm)	Ref.
Cu_xO-CeO_2/Al_2O_3+H_2O_2	/	538	0.629	This work
SiO_2+H_2O_2+TiO_2	Light	107	0.423	[1]
SiO_2+Fe_3O_4+H_2O_2	/	469	2.94	[2]
SiO_2@MnO_2+$KMnO_4$	/	403	0.62	[3]
Diamond+Al_2O_3+Cu+GO/Fe_3O_4+H_2O_2	/	1650	2.2	[4]
TiO_2/NDs/GO+H_2O_2	Light	600	1.170	[5]
Al_2O_3+$NaHCO_3$+H_2O_2	/	220	0.287	[6]
mSiO_2@Cds@CeO_2+H_2O_2+PVP	Light	123	0.211	[7]
Al_2O_3@MnO_2+$KMnO_4$	/	640	0.73	[8]
Diamond+Ag@AgCl+H_2O_2	Light	1757.6	0.45	[9]
GO+Al_2O_3+Fe+H_2O_2	/	700	0.615	[10]
SiO_2+Fe_3O_4+H_2O_2+$NaHCO_3$	Electric	260	0.127	[11]
Al_2O_3+CH_3OH	/	260	0.150	[12]
SiO_2+H_2O_2+TiO_2	Light	4050	1.09	[13]
Cr-SiO_2+$KMnO_4$	/	478	0.51	[14]
Al_2O_3@MIL-100(Fe)	Light	417	2.17	[15]
MRE polishing pad (CIP@Fe_3O_4)	magnetically	1760	0.313	[16]
MRE polishing pad (CIP)	magnetically +Light	5019	0.368	[17]
Fe_3O_4+MoS_2	/	1006	0.215	[18]
Plasma-assisted polishing (PAP)	/		0.26	[19]
ECMP polishing pad (Diamond+Cu)	Electric	1412	5.02	[20]
EDAP+ polishing pad (Diamond+Cu)	Electric	930	0.33	[21]
GO+ H_2O_2+TiO_2+Diamond	Light	1725	1.138	[22]
$FeSO_4$ microcapsules+W0.5 CeO_2	/	2391	0.617	[23]
$BaTiO_3$	Piezo-CMP		0.45	[24]
$BiFeO_3$	Piezo-Fenton	223.6	0.287	[25]
CeO_2@C60	/	334	0.57	[26]
Sodium bismuth titanate nanospheres	Light	154	0.386	[27]
Al_2O_3@MnO	/	640.47	0.73	[28]
CeO_2+ $KMnO_4$+ $NaHCO_3$+PVP	/	646	0.073	[29]
Electrochemical anodization	/	10140	0.34	[30]
Fe-doped CeO_2	Light	114.23		[31]

References

[1] Yan, Q. S.; Wang, X.; Xiong, Q.; Lu, J. B.; Liao, B. T. The influences of technological parameters on the ultraviolet photocatalytic reaction rate and photocatalysis-assisted polishing effect for SiC. *J. Cryst. Growth.* **2020**, 531, 125379-125386.

[2] Shi, D.; Yin, T.; Feng, K. P.; Zhao, T. C. Chemical mechanical polishing for monocrystal SiC assisted by the heterogeneous Sono-Fenton oxidation. *ECS J. Solid State Sci. Technol.* **2024**, 13, 034001-034012.

[3] Yang, R. X.; Lei, H.; Zhang, J. H. Preparation of SiO_2@MnO_2 composite abrasives and their performance in chemical-mechanical polishing of SiC substrates. *Ceram. Int.* **2024**, 50, 34796-34805.

[4] Feng, K. P.; Xu, L. X.; Gu, Y. Z.; Zhao, L.; Zhao, T. C.; Lyu, B. H. Study on material removal mechanism of solid phase Fenton catalytic polishing of SiC wafer with gel-forming abrasive disc. *Mater. Sci. Semicond. Proc.* **2025**, 194, 109488-109501.

[5] Chen, S. D.; Lei, H. Improvement in the planarization of 4H-SiC(0001) achieved by photo-assisted chemical mechanical polishing (P-CMP) using nano TiO_2-based composite abrasive with heterostructure. *Friction.* **2025**, 13, 9440993-9441005.

[6] Shen, Y.; Wang, H. X.; Guo, X. G.; Gao, S. Environment-friendly chemical mechanical polishing using $NaHCO_3$-activated H_2O_2 slurry for highly efficient finishing of 4H-SiC (0001) surface. *J. Manuf. Process.* **2024**, 109, 213-221.

[7] Wang, M. H.; Mu, Z. Y.; Wang, T. Y.; Chen, Y.; Chen, A. L. Double-layered core-shell heterostructures of $mSiO_2$@CdS@CeO_2 abrasive systems toward photochemical mechanical polishing (PCMP) applications. *Appl. Surf. Sci.* **2023**, 614, 156274-156288.

[8] Zhang, P. J.; Lei, H.; Zhang, Z. F.; Zhang, J. H.; Chen, S. D.; Hu, X. G. Synthesis of Al_2O_3@MnO_2 composite abrasives and their chemical mechanical polishing performance on silicon carbide (SiC). *Ceram. Int.* **2024**, 50, 19935-19944.

[9] Lin, C.; Lu, J. B.; Huang, N. Y.; Wu, Q. Y.; Yan, Q. S. Study on process parameters of ultraviolet photocatalytic-Fenton reaction polishing of single-crystal silicon carbide based on Ag@AgCl photocatalyst. *Diam. Relat. Mater.* **2025**, 156, 112400-112410.

[10] Chen, S. D.; Lei, H. Polishing performance and mechanism of a novel Fe-based slurry for chemical mechanical polishing. *Tribol. Int.* **2024**, 194, 109549-109560.

[11] Kang, H. L.; Zhong, M.; Li, X. B.; Yi, M. R.; Chen, J. F.; Xu, W. H. Investigation of Fenton-electrochemical oxidation behavior and polishing mechanism of SiC. *Precis. Eng.* **2025**, 93, 334-343.

[12] Shen, J. F.; Chen, H. B.; Chen, J. P.; Lin, L.; Gu, Y. Y.; Jiang, Z. L.; Li, J.; Sun, T. Mechanistic difference between Si-face and C-face polishing of 4H-SiC substrates in aqueous and non-aqueous slurries. *Ceram. Int.* **2023**, 49, 7274-7283.

[13] Lin, C.; Xie, J. L.; Lu, J. B.; Yan, Q. S. Study on the photocatalytic performance of photocatalytic fixed polishing plate and its effect on the polishing performance of single-crystal SiC. *Mater. Sci. Semicond. Proc.* **2025**, 194, 109556-109569.

[14] Yang, R. X.; Lei, H. Synthesis of peanut-like Cr-SiO_2 composite abrasives and their effects on chemical-mechanical polishing of SiC substrates. *J. Alloys. Compd.* **2025**, 1039, 183252-183261.

[15] Chen, X. Y.; Chen, S. D.; Lei, H. Synthesis of a novel Al_2O_3@MIL-100 (Fe) composite abrasive and its application in 4H-SiC chemical mechanical polishing. *Colloids. Surf. A Physicochem. Eng. Aspects.* **2025**, 725, 137502-137512.

[16] Hu, D.; Liu, K. X.; Xue, E. C.; Chen, L. J.; Lu, J. B. Polishing performance of single-crystal SiC with a magnetically controll-Fenton reaction magnetorheological elastomer pad. *J. Environ. Chem. Eng.* **2026**, 14, 122143-122156.

[17] Li, H. L.; Liang, W. R.; Lu, J. B.; Hu, D.; Huang, Z. R. Mechanism investigation of single-crystal SiC processing using magnetorheological elastomeric polishing pad with UV photocatalytic-Fenton composite reaction. *Mater. Today Commun.* **2025**. 49, 113799-113811.

[18] Li, W. Y.; Lv, G.; Wang, C. W.; Wang, K. Y. Polishing performance and Co-catalytic Fenton mechanism of a novel Fe_3O_4/MoS_2 slurry for silicon carbide wafer chemical mechanical polishing. *Appl. Surf. Sci.* **2026**, 740, 167061-167071.

[19] Han, Y. X.; Luo, C. Y.; Li, X. L.; Wang, X.; Wang, J. H.; Yuan J. L. Insights into the atomic-scale removal mechanism of SiC in plasma-assisted polishing. *Appl. Surf. Sci.* **2026**, 721, 165518-165530.

[20] Luo, Q. F.; Hu, Y. K.; Zhu, Y. Y.; Lu, J.; Ke, C. M.; Huang, H. Preparation and properties of conductive fixed abrasive polishing discs for electrochemical mechanical polishing of SiC substrates. *Mater. Sci. Semicond. Proc.* **2026**, 211, 110710-110718.

[21] Luo, Q. F.; Lv, X. K.; Wang, W. T.; Lu, J.; Wang, N. C.; Ke, C. M.; Jiang, F.; Huang, H. Elucidation of the material removal mechanism of SiC electro-discharge assisted polishing based on conductive polishing pad. *Wear.* **2026**, 601, 206831-206845.

[22] Zhang, Y.; Cao, Z. C.; Miao, Y. W.; Liu, H. T.; Huang, T. Machining characteristics and principle in graphene-oxide-enhanced photocatalysis-assisted polishing of SiC ceramic. *J. Manuf. Process.* **2026**, 164, 19-34.

[23] Xie, J. Z.; Li, Z. H.; Xiong, Y. L.; Ling, H.; Fu, H. Z.; Ou, Y. T.; Luan, T. X.; Wong, M. H.; Pan, J. S. Study on polishing performance of single crystal SiC assisted by $FeSO_4$ microcapsules. *Mater. Sci. Semicond. Proc.* **2026**, 212, 110802-110819.

[24] Hu, T.; Feng, J. X.; Yan, W.; Tian, S. H.; Sun, J. X.; Liu, X. S.; Wei, D.; Wang, Z. M.; Yu, Y.; Lam, J. C.; Liu, S. R.; Wang, Z. L.; Xiong, Y. Piezocatalysis for chemical-mechanical polishing of SiC: dual roles of t-$BaTiO_3$ as a piezocatalyst and an abrasive. *Small.* **2024**, 23, 2310117-2310126.

[25] Liu, K. K.; Chen, G. M.; Ni, Z. F.; Lv, W. J.; Lu, X. Y. $BiFeO_3$ nanoparticles for chemical mechanical polishing of SiC: A piezoelectric-fenton-like synergistic strategy. *ECS J. Solid State Sci. Technol.* **2026**, 15, 034001-034012.

[26] Li, J.; Lei, H.; Zheng, T. C.; Sun, P. X. Synthesis of CeO_2@C_{60} composite abrasives and their performance in the chemical mechanical polishing of SiC. *Mater. Chem. Phys.* **2026**, 362, 132763-132776.

[27] Song, X. Y.; Ni, Z. F.; Lv, W. J.; Lu, X. Y. Sodium bismuth titanate nanospheres as dual-functional photocatalytic abrasives for chemical mechanical polishing of SiC. *Mater. Lett.* **2026**, 417, 140736-140740.

[28] Zhang, P. J.; Lei, H.; Zhang, Z. F.; Zhang, J. H.; Chen, S. D.; Hu, X, G. Synthesis of Al_2O_3@MnO_2 composite abrasives and their chemical mechanical polishing performance on silicon carbide (SiC). *Ceram. Int.* **2024**, 50, 19935-19944.

[29] Song, X.; Zou, Y. R.; Guo, J. N.; Dong, Z. G.; Kang, R. K.; Gao, S. Atomic-level surface formation of large-size SiC substrates by chemical mechanical polishing: interfacial chemistry and removal mechanism. *J. Mater. Chem. C.* **2026**, DOI: 10.1039/D6TC01597B.

[30] Wu, L. W.; Wang, Y. H.; Wei, M.; Shen, M. M.; Wang, Y. G.; Chen, H. Y.; Lyu, B. H.; Hang, W. Study on the mechanism of electrochemical anodization for the fixed-abrasive polishing of 4H-SiC. *ECS J. Solid State Sci. Technol.* **2026**, 15, 034003-034015.
[31] Xu, N.; Gao, Z. H.; Huo, Y.; Gao, K. L.; Wang, Y. S.; Zhang, G. S.; Lin, Y.; Wang, Z. Dual-pathway mechanism of Fe-doped CeO_2 abrasives in photo-Fenton-assisted CMP of SiC, *J. Rare Earths.* **2026**, DOI: 10.1016/j.jre.2026.02.005.